Ontogenic changes in hematopoietic hierarchy determine pediatric specificity and disease phenotype in fusion oncogene-driven myeloid leukemia

Cécile K. Lopez[1,2,3,4], Esteve Noguera[1,2,4,#], Vaia Stavropoulou[5,#], Elie Robert[1,2,4,#], Zakia Aid[1,2,4], Paola Ballerini[6], Chrystèle Bilhou-Nabera[7], Hélène Lapillonne[7], Fabien Boudia[1,2,4,9], Cécile Thirant[1,2,4], Alexandre Fagnan[1,2,4,9], Marie-Laure Arcangeli[10], Sarah J. Kinston[11], M'Boyba Diop[2], Bastien Job[2], Yann Lecluse[2], Erika Brunet[12], Loélia Babin[12], Jean-Luc Villeval[1,2], Eric Delabesse[13], Antoine H.F.M. Peters[14], William Vainchenker[1,2], Muriel Gaudry[1,2], Riccardo Masetti[15], Franco Locatelli[16], Sébastien Malinge[1,2,3,4], Claus Nerlov[17], Nathalie Droin[1], Camille Lobry[1], Isabelle Godin[1,2], Olivier A. Bernard[1,2,3,4], Berthold Göttgens[11], Arnaud Petit[6], Françoise Pflumio[10], Juerg Schwaller[5,*], Thomas Mercher[1,2,4,9,*]

[1]INSERM U1170, Gustave Roussy, 94800 Villejuif, France
[2]Gustave Roussy, 94800 Villejuif, France
[3]Université Paris-Saclay, 94800 Villejuif, France
[4]Equipe labellisée Ligue Nationale Contre le Cancer, 75013 Paris, France
[5]University Children's Hospital Beider Basel (UKBB) and Department of Biomedicine, University of Basel, 4031 Basel, Switzerland
[6]Hôpital Trousseau, AP-HP, 75012 Paris, France
[7]Sorbonne Université, CRSA – Unité INSERM, AP-HP, Hôpital Trousseau, F-75012 Paris, France
[8]Hôpital Saint Antoine, AP-HP, 75012 Paris, France
[9]Université Paris Diderot, 75013 Paris, France
[10]Unité Mixte de Recherche 967 Inserm-CEA/DRF/IBFJ/IRCM/LSHL- Université Paris-Diderot-Université Paris-Sud, Equipe labellisée Association Recherche contre le Cancer, 92265 Fontenay-aux-Roses Cedex, France
[11]Wellcome and MRC Cambridge Stem Cell Institute and the Cambridge Institute for Medical Research, University of Cambridge, Cambridge, UK.
[12]Genome Dynamics in the Immune System Laboratory, Institut Imagine, INSERM, UMR 1163, Université Paris Descartes, Sorbonne Paris Cité, Equipe Labellisée Ligue Contre le Cancer, 75015 Paris, France.
[13]INSERM U1037, Team 16, Center of Research of Cancerology of Toulouse, Hematology laboratory, IUCT-Oncopole, France
[14]Friedrich Miescher Institute for Biomedical Research (FMI), 4058 Basel, Switzerland; Faculty of Sciences, University of Basel, 4056 Basel, Switzerland.
[15]Department of Pediatrics, "Lalla Seràgnoli", Hematology-Oncology Unit, Sant'Orsola-Malpighi Hospital, University of Bologna, Via Massarenti 11, 40137, Bologna, Italy.
[16]Department of Pediatrics - Sapienza - University of Rome, Hematology-Oncology - IRCCS Ospedale Bambino Gesù - Rome, Italy
[17]MRC Molecular Hematology Unit, MRC Weatherall Institute of Molecular Medicine, Radcliffe Department of Medicine, University of Oxford, Oxford OX3 9DS, UK
[#]Co-second author

*Correspondence:
Thomas Mercher
Institut Gustave Roussy, INSERM U1170
39 rue Camille Desmoulins, 94800 Villejuif
Phone: +33 1 42 11 44 83
E-mail: thomas.mercher@inserm.fr

or
Juerg Schwaller
University Children's Hospital Basel (UKBB)
Department of Biomedicine (DBM), University of Basel
ZLF-Lab 202
Hebelstrasse 20
CH-4031 Basel, Switzerland
Phone: +41 61 265 3504
E-mail: j.schwaller@unibas.ch

KEYWORDS:

Leukemia; pediatric; hematopoietic stem cell; HSC; stemness; primitive hematopoiesis; progenitor cell; cellular identity; self-renewal; transcription factor; single cell transcriptome; gene regulatory network; network inference; physiological model, inducible; megakaryocyte; myeloid; patient-derived xenograft; PDX; childhood; AML-M7; AMKL; CEBPA; GATA1; ERG; ETO2; GLIS2.

ABSTRACT

Fusion oncogenes are prevalent in several pediatric cancers, yet little is known about the specific associations between age and phenotype. We observed that fusion oncogenes, like ETO2-GLIS2, are associated with acute megakaryoblastic or other myeloid leukemia subtypes in an age-dependent manner. Analysis of a novel inducible transgenic mouse model showed that ETO2-GLIS2 expression in fetal hematopoietic stem cells induced rapid megakaryoblastic leukemia while expression in adult bone marrow hematopoietic stem cells resulted in a shift toward myeloid transformation with a strikingly delayed *in vivo* leukemogenic potential. Chromatin accessibility and single cell transcriptome analyses indicate ontogeny-dependent intrinsic and ETO2-GLIS2-induced differences in key transcription factor activities, including ERG, SPI1, GATA1 and CEBPA. Importantly, switching off the fusion oncogene restored terminal differentiation of the leukemic blasts. Together, these data show that aggressiveness and phenotypes in pediatric acute myeloid leukemia result from an ontogeny-related differential susceptibility to transformation by fusion oncogenes.

SIGNIFICANCE

This work demonstrates that the clinical phenotype of pediatric acute myeloid leukemia is determined by ontogeny-dependent susceptibility for transformation by oncogenic fusion genes. The phenotype is maintained by potentially reversible alteration of key transcription factors indicating that targeting of the fusions may overcome the differentiation blockage and revert the leukemic state.

INTRODUCTION

Increasing evidences support a correlation between age, driver oncogene and disease phenotype in pediatric cancers (1,2). The differences between adult and pediatric cancers may stem from either the distinct properties of the driver oncogenes or inherent differences between fetal and adult tissue. In acute leukemia, some fusions oncogenes are acquired *in utero* and are diagnosed almost exclusively during childhood (3–5) for which efficient leukemogenesis models are lacking (6). Childhood *de novo* acute megakaryoblastic leukemia (AMKL) is an aggressive subtype of acute myeloid leukemia (AML) that harbors recurrent fusion oncogenes (e.g. ETO2-GLIS2, OTT-MAL, NUP98-KDM5A)(7–10). Intriguingly, several AMKL fusions are also detected in patients with other AML subtypes (8,11,12), although the determinants of the genotype/phenotype association remain unknown. Similarly to other aggressive childhood cancers such as Ewing sarcoma (13), these fusions are rarely associated with additional recurrent mutations in patients (9,14) and they strongly impact the epigenome (15,16), thereby suggesting that global transcriptional deregulation is sufficient to drive the disease and a likely candidate for direct therapeutic targeting (17,18). Nevertheless, these cancers currently lack adequate animal models that precisely recapitulate the characteristics of the disease observed in patients. Such models could provide mechanistic insights to understand pediatric cancer specificity.

Several differences between fetal and adult normal hematopoiesis exist (19,20). In adults, hematopoietic stem cells (HSC) are at the top of a hierarchy and differentiate toward more committed progenitors to generate the mature blood cell types. Although the precise trajectories that govern normal hematopoiesis remain a matter of debate (21–24), leukemogenic processes are strongly influenced by the type of cell targeted by fusion oncogenes (25). A recent study has proposed that fetal liver (FL) hematopoiesis primarily involves multipotent progenitors, while adult hematopoiesis is chiefly regulated by committed progenitors with more restricted lineage potentials (26). This view is largely supported by single cell transcriptome data showing that most adult hematopoietic progenitors present signs of lineage commitment (27–29,24,21). At the molecular level, fetal and adult hematopoiesis present differential activity of LIN28B (30–33), GATA factors-regulated Polycomb complexes (34) and CEBPA/MYCN transcription factors (35).

To better understand the genotype/phenotype association in pediatric cancers, we investigated how the fetal and adult cellular architectures (22–24,36,27) impact the transformation and disease phenotype driven by ETO2-GLIS2 (hereafter abbreviated EG). We developed an inducible transgenic mouse model that efficiently phenocopied the human

disease with striking differences in latency, phenotype and molecular wiring, depending on the ontogenic stage at which the driver fusion oncogene is activated.

RESULTS

AMKL is diagnosed at a younger age than AML in pediatric patients

We first screened a cohort of 276 pediatric leukemia patients (37) for the presence of *EG* and confirmed that *EG* occurred in AMKL patients and other AML (AML-M0 to AML-M5) subtypes (12), with an overall incidence of 4.7% (Fig. 1A, B, Supplementary Table S1). The overall survival was poor for all patients with a trend towards a worse prognosis for those presenting with an AMKL phenotype (Supplementary Fig. S1A). In addition to the known EG^+ MO7e megakaryoblastic cell line, we found that the CMS leukemia cell line was also EG^+ and presented with a myeloid phenotype (Supplementary Fig. S1B-E). Strikingly, EG^+ AMKL patients were diagnosed at a significantly younger age of (1.66±0.18 years [n=33]) compared with other EG^+ AML patients (8.53±1.73 years [n=15]; $p<0.0001$)(Fig. 1C). A similar trend was observed in AMKL patients carrying either NUP98-KDM5A (Fig. 1D) or MLL fusions (Fig. 1E) as well as for all AMKL patients regardless of the genetic subgroup (Fig. 1F).

We applied patient-derived xenografts (PDX)(8) to expand EG^+ AMKL and EG^+ AML cells in immunodeficient mice. Overall, 3/5 EG^+ AMKL and 2/8 EG^+ AML transplants successfully engrafted (Supplementary Table S1). While AMKL xenografts generally expressed the megakaryoblastic marker $CD41^+$ but not the myeloid marker $CD15^-$ (as observed for patient #13), AML blasts were $CD15^+CD41^-$ (e.g. patient #7)(Fig. 1G). Interestingly, we identified a six-year-old EG^+ patient (#5) diagnosed as AML-M2, who presented with immature blasts ($CD34^+CD15^-CD41^-$) and two smaller cellular fractions ($CD34^+CD41^+CD15^-$ or $CD34^+CD41^-CD15^+$)(Fig. 1G). All cell populations presented with distinct morphologies (Fig. 1H,I) and expressed *EG* (Supplementary Fig. S1F). Upon injection of the three flow-purified cell populations into secondary recipients, only the immature $CD34^+CD41^-CD15^-$ cell population successfully engrafted into recipients (Fig. 1J) and regenerated the three populations (Fig. 1K), thereby indicating dual megakaryoblastic and myeloid differentiation.

Together, these results show that pediatric AMKL occurs at a significantly younger age than other AML subtypes irrespective of the driver oncogene. Importantly, the dual megakaryoblastic/myeloid phenotype in the EG^+ patient indicates that AMKL-associated fusion oncogenes can transform HSC or multipotent progenitors.

ETO2-GLIS2 efficiently induces leukemia in mice

To analyze the determinants of EG-driven leukemogenesis and the associated megakaryoblastic and myeloid phenotypes, we established a doxycycline (Dox)-regulated

transgenic mouse model (Supplementary Fig. S2A). Hereby, EG expression is controlled by a reverse tetracycline-controlled transactivator (rtTA) integrated into the *Rosa26* gene locus, and results in similar EG expression levels as observed in AMKL patient blasts (Supplementary Fig. S2B-C). To assess the consequences of EG expression, we continuously exposed double transgenic *iEG:rtTA* females (hereafter abbreviated iEG) to Dox (Dox^+, Fig. 2A). Although most hematological parameters remained unchanged at six weeks post-induction (data not shown), iEG animals consistently presented with an abnormal bone marrow (BM) $Lin^-CD150^-Kit^+CD41^+$ cell population (Supplementary Fig. S2D) bearing a myeloid and megakaryoblastic clonogenic potential in methylcellulose cultures (Supplementary Fig. S2E). Later, Dox-treated iEG animals developed lethal hematological malignancies with a prevalence of 96.9% (31/32 mice, Supplementary Fig. S2F), which was classified into two groups based on the most abundant blast populations (Fig. 2B, C, Supplementary Fig. S2G). Approximately 20% of the mice (4/19, Group 1) presented with a $CD41^+$ (megakaryoblastic) phenotype with a median latency of 164 days (Fig. 2D). Group 2 presented with heterogenous phenotypes ranging from predominantly Kit^+ (immature) with low number of $CD11b^+Gr1^+$ (myeloid) cells to predominantly maturing Kit^- $CD11b^+Gr1^+$ myeloid features after a median latency of 251 days (Fig. 2B-D, Supplementary Fig. S2G). Histological analyses revealed altered spleen architectures and confirmed that BM and spleens from Group 1 mice were infiltrated with immature von Willebrand factor (VWF^+) megakaryoblasts, while Group 2 presented with myeloid features in the BM and extramedullary hematopoiesis in the spleen (Fig. 2C, Supplementary Fig. S2H). All diseased mice developed hepatosplenomegaly (Fig. 2E) and anemia (Fig. 2F) and Group 1 was associated with significantly higher white blood cell (WBC) counts (Fig. 2F). The cell-autonomous nature of the disease and its dependence on EG expression was demonstrated by transplantation of BM cells into Dox^+ wild-type (WT) recipients that developed disease after a shorter mean latency (120 days), while Dox^- recipients never developed any disease (Fig. 2G-J, Supplementary Fig. S2H). Collectively, this inducible transgenic model faithfully recapitulates EG^+ leukemia development as observed in patients.

Developmental stage determines the phenotype of ETO2-GLIS2$^+$ leukemia

To investigate the impact of the developmental stage, we induced iEG expression in Lin^- hematopoietic stem and progenitor cells (HSPC) obtained from fetal liver (FL) at embryonic day (E) 12.5, newborn BM (1-2 weeks old) and adult BM (ABM, 8 weeks old) (Fig. 3A). *In vitro*, iEG expression significantly increased the clonogenic activity with passages in all contexts (Fig. 3B). While iEG^+ FL-derived cells homogeneously expressed CD41, iEG^+ ABM-derived cells also consistently showed a $CD11b^+Gr1^+$ myeloid phenotype (Fig. 3C, Supplementary Fig. S3A). Newborn-derived iEG cells presented with a myelo/megakaryoblastic intermediate phenotype between that of FL and ABM. Similar results were obtained upon retroviral

expression of EG in WT cells (Supplementary Fig. S3B). These data indicate that fetal hematopoiesis favors EG-induced megakaryoblastic transformation *in vitro*.

To compare the capacity of FL- and ABM-derived iEG cells to develop disease, we transplanted $1x10^6$ mononuclear iEG cells from E14.5 FL or ABM donors (carrying a ubiquitously-expressed GFP reporter to track their progeny) donors into Dox^+ WT recipients (Fig. 3A). Mice engrafted with iEG FL cells developed lethal leukemia with median latency (39 days)(Fig. 3D) characterized by splenomegaly, high WBC, anemia, thrombocytopenia, and infiltration with $CD41^+$ megakaryoblasts in several organs, while mice engrafted with iEG ABM cells developed the disease after a significantly prolonged latency (median 397 days, p=0.0008) associated with heterogenous phenotypes ranging from Kit^+CD41^- immature to predominantly $CD11b^+Gr1^+$ myeloid features (Fig. 3D-H and data not shown). To address the consequences of EG expression on fetal progenitors *in vivo*, we exposed pregnant females (E13) to Dox and analyzed the embryos 36 hours later. All iEG-expressing embryos showed gross morphological and hematological abnormalities (Fig. 3I), with decreased erythroid and myeloid cells and increased megakaryoblastic progenitors (Fig. 3J).

Taken together, these observations show that the developmental stage determines the predominance of aggressive megakaryoblastic over myeloid leukemia upon ETO2-GLIS2 expression.

ETO2-GLIS2 expression in fetal LT-HSC induces a megakaryoblastic phenotype

To address the consequence of EG on distinct populations of the hematopoietic hierarchy, we purified control (CTRL) and iEG long-term HSC (LT-HSC) and multipotent progenitors (MPP2, MPP3 and MPP4)(38) obtained from E14.5 FL or ABM (Supplementary Fig. S3C) and characterized their clonogenic and phenotypic profile in Dox^+ methylcellulose cultures (Fig 4A). CTRL FL LT-HSC and MPP generated both myeloid $Gr1^+$ and megakaryoblastic $CD41^+$ cells (Fig. 4B, Supplementary Fig. S3D), thereby confirming that most normal mouse FL progenitors maintain a megakaryoblastic potential as observed in humans (26). iEG FL LT-HSC and MPP2 cells exclusively generated $CD41^+$ cells (Fig. 4B, Supplementary Fig. S3D), MPP3 cells yielded a large majority of $CD41^+$ cells and rare $Gr1^+$ myeloid cells (Fig. 4B, Supplementary Fig. S3D), and MPP4 cells did not significantly form any colony (Supplementary Fig. S3E). iEG FL LT-HSC and MPP2/3 cells showed increased replating activity compared with CTRL (Fig. 4C). To define the differentiation potential of iEG-transformed cells, iEG FL LT-HSC and MPP2/3 cells derived from the fourth plating were cultured without Dox (Fig. 4A), which resulted in myeloid and megakaryoblastic differentiation respectively (Fig. 4D, Supplementary Fig. S3F). $CD41^+$ and $Gr1^+$ iEG cell lines could be derived after flow purification and long-term cultures (Supplementary Fig. S3H) and their $CD41^+$ megakaryoblastic phenotype correlated with the high presence of Dox (Supplementary Fig. S3I). Consistently, higher *ETO2-GLIS2* expression

was observed in AMKL vs. AML patient blasts (Supplementary Fig. S1G), supporting the importance of EG dosage as shown for other fusion oncogenes (39).

Using ABM cells, CTRL LT-HSC formed $Gr1^+$ and $CD41^+$ cells (Fig. 4E, F), whereas CTRL MPP2/3/4 cells generated almost exclusively $Gr1^+$ cells (Fig. 4F, Supplementary Fig. S3D), indicating that the megakaryoblastic potential is qualitatively and quantitatively lower in ABM than in FL (Supplementary Fig. S3G). By contrast, iEG ABM LT-HSC gave rise almost exclusively to $CD41^+$ cells, while MPP2/3/4 cells generated $CD11b^+Gr1^+$ myeloid cells with a higher proportion than iEG FL MPP (Fig. 4F, Supplementary Fig. S3D). While iEG FL MPP4 cells did not generate colonies, iEG ABM MPP4 cells showed increasing clonogenic activity upon serial replatings and a myeloid morphology (Fig. 4F-H).

We next investigated whether iEG endows single LT-HSC or MPP3 cells with dual myeloid/megakaryoblastic phenotypic potential as observed in patient #5 (Fig. 1G). The majority (56%) of CTRL ABM LT-HSC-derived cells showed a dual phenotype, while others showed either megakaryoblastic or myeloid phenotypes. Upon iEG induction, ABM LT-HSC formed primarily megakaryoblastic colonies (89%) with only a few dual phenotype colonies (11%)(Fig. 4I, J, Supplementary Fig. S3J). While CTRL MPP3 cells exclusively generated myeloid cells under these conditions, 48% of iEG MPP3 cells yielded a dual megakaryoblastic and myeloid profile, thereby indicating that EG imposes megakaryoblastic as well as dual myeloid/megakaryocytic potential on single MPP3 progenitors.

Collectively, these data show that murine FL HSPC present a higher susceptibility to megakaryoblastic transformation by EG than ABM HSPC. They also demonstrate that EG expression in ABM LT-HSC results in an exclusively megakaryoblastic phenotype, while expression in further committed progenitors is required for myeloid transformation.

ETO2-GLIS2 alters the LT-HSC transcriptional network in an ontogeny-dependent manner

To compare the molecular consequences of EG expression in different developmental (FL vs. ABM LT-HSC) or hierarchical (LT-HSC vs. MPP4 ABM cells) contexts, we performed single cell RNAseq (scRNAseq) on these purified populations after a 24-hour Dox induction in CTRL and iEG cells. Clustering and differential expression analyses revealed that iEG impacted FL LT-HSC transcriptome more than those from ABM LT-HSC (3772 vs. 151 differentially-expressed genes, respectively) or MPP4 (only 3 differentially-expressed genes) (Fig. 5A, Supplementary S4A-C, Supplementary Tables 2-4). Previously defined signatures of upregulated ("Up") genes in ETO2-GLIS2$^+$ AMKL patients (40,41) were enriched in iEG$^+$ LT-HSC derived from both FL and ABM contexts. However, the signature of downregulated ("Down") genes in ETO2-GLIS2$^+$ AMKL patients was only deregulated in FL LT-HSC (Fig. 5B, Supplementary Fig S4D). iEG MPP4 cells showed few differentially expressed genes and no

enrichment for EG^+ AMKL patient signatures (Supplementary Fig. S4D). These data show that the iEG signature obtained in FL LT-HSC better recapitulates the molecular consequences observed in EG^+ AMKL patients than the signatures observed in ABM LT-HSC or MPP4.

GSEA showed enrichment of stem cell signatures in both fetal and adult iEG LT-HSC (e.g. *Myct1*, *Esam*), significantly more pronounced for several genes in fetal LT-HSC (e.g. *Vwf* and *Hlf*)(Fig. 5C, D, Supplementary Fig. S4E, F). Expression signatures from progenitors and more mature populations (e.g. MPP3, MPP4, Monocytes, Neutrophils, Megakaryocytes) were significantly downregulated in FL LT-HSC compared to adult LT-HSC with a lower expression of myeloid (e.g. *Spi1*), erythroid (e.g. *Nfe2)* and megakaryocytic genes (e.g. *Mpl*) (Fig. 5C, E, Supplementary Fig. S4E), supporting a more pronounced blockage of differentiation in FL LT-HSC.

To investigate related transcription factor (TF) activities, network inference and activity prediction with ARACNe and VIPER programs was used (Supplementary Fig. S5A, Supplementary Tables S5-7). This first confirmed a higher expression level and activity of EG in iEG^+ cells on Dox (Supplementary Fig. S5B). For several key TF, it also predicted significantly different activities without significant difference in mRNA expression (Supplementary Fig. S5C, Supplementary Tables S8-9). Accordingly, activity-based clustering confirmed that iEG expression impacted adult LT-HSC more than MPP4 cells (Supplementary Fig. S5D). Several TFs know to act as oncogenes or cofactors (e.g. ERG, HLF, MECOM, HOXA10, MEIS1) presented increased activities, while other key differentiation TF were downregulated (RBM15, SPI1, CEBPA) (Supplementary Fig. S5E).

To investigate the association between transcriptional changes and chromatin remodeling, we mapped open chromatin regions by ATAC-seq in FL progenitors 24 hours after EG induction. Most open chromatin regions were common between CTRL and iEG (33,429 peaks), while some were lost/decreased (12,412 Down peaks) or acquired/increased (5,975 Up peaks) in iEG cells (Fig. 5F, G, I). Notably, 29% of the genes deregulated in scRNAseq analyses showed differential ATAC-seq peaks around the genes' loci, suggesting that the transcriptional modifications induced by EG are partly due to chromatin remodeling (Fig. 5H). ATAC-seq also revealed differences between the $CD41^+$ and $Gr1^+$ iEG cell lines with $Gr1^+$ cells showing mostly chromatin closing as compared to wild-type FL (1,899 Up and 16,383 Down peaks), while $CD41^+$ cells showing more chromatin opening (34,167 Up and 19,971 Down peaks) (Fig. 5I). Notably, the regions opened by iEG in FL progenitors (5,975 Up peaks) at 24h were also enriched in $CD41^+$ but not in $Gr1^+$ cells, suggesting a closer proximity between iEG FL and $CD41^+$ than with myeloid transformed cells (Fig. 5J).

Motif analysis within the ETO2-GLIS2-specific gained open regions (Up peaks) showed a lower representation of GATA motifs and an increased representation of ETS/ERG motifs (Fig. 5K) in FL progenitors, in $CD41^+$ and in $Gr1^+$ cell lines compared to their representation within

regions specific for the control cells (Down peaks). Interestingly, motifs of some key myeloid transcription factors, including SPI and CEBP, were significantly enriched only in $Gr1^+$ transformed cell, supporting a role for these factors in the transcriptional regulation in myeloid $ETO2\text{-}GLIS2^+$ cells.

Together, these data show that EG imposes more prominent transcriptional changes in fetal liver-derived than in adult HSC, in part, through rapid changes in chromatin accessibility to regions presenting binding sites for major hematopoietic transcription factors including GATA, ETS and CEBPA.

GATA1 and CEBPA activities correlate with pediatric AML phenotypes

HSC lineage specification involves TF expression or activity switches, including a SPI1/CEBPA module directing myeloid development (42,43) and an ERG/GATA1 balance (44) regulating the megakaryocytic fate and altered in human AMKL (10). As these TF are also involved in hematopoietic ontogeny (34,35), we investigated TF expression and functional contribution to EG-induced megakaryoblastic and myeloid phenotypes. Wild-type (CTRL) FL HSPC expressed more *Gata1*, *Erg* and *Spi1* and less *Cebpa* than their ABM counterparts. Twenty-four hours after iEG induction, all genes were downregulated excepted *Erg* in FL HSPC. However, iEG FL HSPC expressed significantly higher levels of *Gata1* and *Erg* and lower levels of *Cebpa* and *Spi1* than iEG ABM HSPC (Fig. 6A). Notably, *Spi1* was more strongly downregulated by iEG in FL (4.9-fold) than in adult (2.2-fold) progenitors, consistently with scRNAseq data performed in purified LT-HSC (Fig. 5E). We then quantified expression of these TF in CTRL and iEG ABM LT-HSC- and MPP4-cells. *Erg* and *Gata1* were more expressed in iEG LT-HSC-derived cells than in iEG MPP4-derived cells, while *Cebpa* and *Spi1* were highly expressed in MPP4 cultures (Fig. 6B). We then functionally assessed whether increasing ERG or GATA1 activity may impose a megakaryoblastic phenotype in iEG MPP4 cells and whether increasing SPI1 or CEBPA activity biased iEG LT-HSC toward a myeloid phenotype (Fig. 6C-E). Retroviral GATA1, and to a lesser extent ERG, expression enhanced the megakaryocyte phenotype in iEG MPP4 cells. In iEG LT-HSC, expression of CEBPA, but not SPI1, enhanced the myeloid phenotype.

We then compared *ERG*, *GATA1*, *SPI1* and *CEBPA* expression levels in leukemic blasts from AMKL and AML patients and in different populations from the dual AML/AMKL phenotype patient (#5) (Fig. 6F and Supplementary Fig. S6A). AMKL cases showed high *ERG* and *GATA1* and low *SPI1* and *CEBPA* expression, while AML cases presented an opposite expression pattern. Similar profiles were observed in the human EG^+ cell lines MO7e (AMKL) and CMS (AML) (Supplementary Fig. S1E). The EG^+ case with a dual phenotype (#5) showed an intermediate expression of *CEBPA*, *GATA1* and *ERG* compared to AMKL and AML patients (Fig. 6F). In this patient, the most immature $CD34^+CD41^-CD15^-$ blasts showed the highest

ERG expression compared to $CD41^+$ and $CD15^+$ blasts, while the $CD41^+$ blasts showed the highest *GATA1* expression and the $CD15^+$ blasts showed the highest *SPI1* expression levels. Notably, $CD41^+$ blasts showed an unexpected combination of $GATA1^{high}$ and $CEBPA^{high}$ expression (Supplementary Fig. S6A), which significance for this peculiar case of dual megakaryoblastic/myeloid phenotype remains to be understood.

Collectively, these data support the idea that the specific association between EG^+ AMKL and young children results from a combination of at least two parameters (Fig. 6G). First, intrinsic differences in the GATA1 and CEBPA activities observed during the normal ontogeny (FL HSC vs. ABM HSC) and in the normal HSPC hierarchy (HSC vs. MPP) are conserved upon EG expression and correlate with the megakaryoblastic/myeloid phenotypic output, respectively. Second, EG induces a stronger deregulation of self-renewal-associated genes (e.g. *ERG* and *SPI1*) in the fetal vs. adult HSC.

ETO2-GLIS2 reversibly transforms LT-HSC

As our cellular and molecular observations indicate that EG hijacks of HSC properties, we compared the *in vivo* leukemogenic potential of purified cell populations and assessed its potential reversibility by tracking the differentiation potential of iEG-transformed cells (carrying the GFP reporter gene) after Dox removal.

GFP^+ FL LT-HSC and MPP3 from E14.5 iEG embryos, or LT-HSC and MPP cells from iEG ABM were transplanted into Dox-treated WT recipients (Fig. 7A). The iEG FL LT-HSC and MPP3 recipients developed fully penetrant and rapid (median: 27 days and 33 days) lethal leukemia (Fig. 7B). The iEG ABM LT-HSC recipients developed disease after a strikingly longer latency (median: 312 days, p=0.017) (Fig. 7B, C, Supplementary Fig. S6B). Only 1 out of 9 iEG ABM MPP3 recipients developed disease with a long latency and none of the iEG ABM MPP4 developed any disease (Fig. 7C, Supplementary Fig. S6B). The FL iEG LT-HSC and MPP3 recipients presented with a more severe disease than the ABM iEG LT-HSC mice as assessed by greater degree of splenomegaly, higher white blood counts, higher percentage of $CD41^+$ cells and lower platelet counts, maturing myeloid populations and lymphoid cells in BM and spleen (Fig. 7D-G). Histological analyses showed that the BM, spleen and liver were infiltrated with GFP^+ cells that were weakly VWF^+. The iEG ABM LT-HSC recipients displayed rare maturing VWF^+ megakaryocytes that were all GFP^-, which was not observed in the iEG FL LT-HSC counterparts (Supplementary Fig. S6C, data not shown).

To investigate the differentiation potential of LT-HSC-derived iEG leukemic cells, we purified the immature $CD41^+CD11b^-Gr1^-$ blasts from iEG FL LT-HSC diseased recipients and grew them in cultures in absence of Dox. As compared with the immature blasts maintained with Dox, they generated both maturing $CD41^+CD42^+$ megakaryocytes and $CD11b^+Gr1^+$ myeloid cells (Supplementary Fig. S6D). This was associated with reduced expression of *iEG* and its

known target *Erg,* while *Gata1* expression increased, consistent with broad differentiation capacities (Supplementary Fig. S6E). To assess long-term hematopoietic potential, BM cells from the ABM LT-HSC-engrafted diseased recipients were transferred into secondary Dox-treated recipients (Fig. 7H). Two weeks post-transplant (=D0 time point), when recipients showed the first signs of disease (Supplementary Fig. S6F, G), some recipients were maintained on Dox (Group A) while Dox-treatment was ceased in group B. At three days after Dox-removal, the platelets counts were back to normal in group B; 80% of platelets originated from iEG-transformed cells as shown by GFP expression (Fig. 7I). GFP^+ cells were also detected later in RBC and WBC (Fig. 7I, Supplementary Fig. S6H). Notably, Dox-treated mice (group A) develop lethal leukemia similar to primary mice while group B off Dox did not (Dox^+, Fig. 7J). Analysis of group B at six-months post Dox removal demonstrated that GFP^+ cells where still present in all analyzed hematopoietic compartments, including mature B and T cells (Fig. 7K, Supplementary Fig. S6I). Together, these data show that iEG expression in FL LT-HSC results in a rapid and aggressive AMKL *in vivo* associated with maintenance of long-term HSC-like differentiation potential once the driver oncogene is switched off.

MLL-AF9 expression in fetal liver LT-HSC induces megakaryoblastic features

In addition to ETO2-GLIS2, other fusion oncogenes, including MLL-AF9, are found in both pediatric AML and AMKL. However, published murine models only displayed MLL-AF9-driven myeloid, but not megakaryoblastic leukemic phenotypes. To assess whether the ontogenic stage and cell hierarchy also affects the phenotype induced by MLL-AF9, we retrovirally expressed MLL-AF9 (rMLL-AF9) in FL- and ABM-derived HSPC from WT mice. Notably, rMLL-AF9 resulted in an increased $CD41^+$ megakaryoblastic phenotype in FL compared to ABM cells (Supplementary Fig. S7A). Next, we transduced purified FL LT-HSC and MPP populations and observed an increased the $CD41^+$ output only with LT-HSC (Supplementary Fig. S7B). Transplantation of rMLL-AF9-transduced cells revealed disease development in both cases presenting with clear $CD41^+$ and VWF^+ megakaryoblastic features only in recipients of FL LT-HSC, but not MPP4 cells (Supplementary Fig. S7C, D). rMLL-AF9-expressing $CD41^+$ blasts also expressed high *Gata1* and low *Spi1* and *Cebpa* expression, while MPP4-derived myeloid blasts showed a mirrored expression pattern (Supplementary Fig. S7E). Collectively, these observations indicate that ontogenic changes in the cellular hierarchy impact disease phenotypes not only for ETO2-GLIS2 but also for other AMKL-associated fusion oncogenes like MLL-AF9.

DISCUSSION

In toto, our observations in patient samples and in inducible transgenic mouse models for pediatric leukemia-associated fusion oncogenes, including ETO2-GLIS2 and MLL-AF9, provide experimental evidence that aggressive pediatric AMKL originates in fetal HSPC and, more globally, that age and phenotype-specific associations observed in human patients rely on changes in the cellular architecture during hematopoietic ontogeny.

A novel inducible transgenic mouse model allowed us to demonstrated that expression of EG in fetal progenitors and adult LT-HSC, but not in further committed adult progenitors, resulted in leukemogenesis *in vivo*. The previous lack of *in vivo* transformation (Dang et al., 2017; Gruber et al., 2012, and our unpublished data) could therefore be due to a poor targeting of LT-HSC by retroviral transduction. The inducible model was also instrumental in demonstrating that HSC-derived EG^+ leukemic cells can maintain long-term reconstitution and differentiation properties upon withdrawal of the driver oncogene. In adult hematopoiesis, several cellular and gene expression studies have indicated the close proximity between LT-HSC and megakaryocytic states in normal and stress conditions (22–24,29,46,47), thus prompting the hypothesis that megakaryopoiesis may represent the native differentiation pathway for LT-HSC (24). Our data indicate that EG alters master hematopoietic TF activities in LT-HSC (e.g. ERG, HLF, MECOM and HOX-related factors) toward a megakaryoblastic state and therefore strongly suggest that EG^+ AMKL is mostly a LT-HSC disease. In addition, expression of MLL-AF9 in fetal LT-HSC led to clear megakaryoblastic features as opposed to fetal MPP or adult progenitors that generated the typical MLL-AF9 myeloid leukemia. Also, other AMKL fusion involves transcription regulators important for both normal HSC and megakaryocyte biology (e.g. OTT1/RBM15)(48). Therefore, we propose a conceptual framework for pediatric AMKL in general in which transcriptional constraints, imposed by distinct oncogenes, represent molecular switches that functionally converge on an early alteration of fetal LT-HSC as they engage the native megakaryocytic differentiation pathway.

This study also demonstrates that the transforming potential of pediatric oncogenes is dependent on the ontogeny-related dynamics of the hematopoietic tissue architecture. Indeed, in our model, iEG expression in fetal LT-HSC generated an aggressive and phenotypically homogeneous megakaryoblastic phenotype, while expression in adult LT-HSC resulted in the development of more heterogeneous phenotypes with delayed latencies. This is consistent with recent findings that normal fetal hematopoiesis is primarily controlled by multipotent HSPC (endowed with megakaryocytic potential), while adult hematopoiesis presents with a higher ratio of committed progenitors (lacking megakaryocytic potential)(26). Molecularly, our data indicate that, while *GATA1* and *CEBPA* expression are both low in EG^+ leukemia, their relative activities may contribute to the megakaryoblastic vs. myeloid phenotype of EG^+ leukemia,

respectively. EG imposed higher *Erg* and lower *Spi1* levels in fetal than in adult LT-HSC, but engineered expression of these factors did not drastically impact the EG-induced phenotype in vitro. Notably, the precise expression level of *Erg* and *Spi1* controlled self-renewal and transformation in other models (49–51). Together, we propose that the association between EG^+ AMKL and the young age of the patients results from the combination of 1-intrinsic differences between normal fetal and adult hematopoiesis together with 2-a stronger alteration of fetal HSC transcriptional regulation by EG, leading to a higher susceptibility of fetal HSC to transformation by EG (Fig. 6G). The former includes a higher proportion of multipotent vs. myeloid-committed progenitors and a higher GATA1 vs. CEBPA activity in fetal as compared to adult stages. The latter includes more a prominent deregulation by EG of a self-renewal module (e.g. ERG and SPI1). As low *CEBPA* activity was also associated with increased competitive advantage and proliferation (35,52), the lower *CEBPA* expression in the EG^+ fetal context may also contribute to the more aggressive leukemia obtained upon EG expression in fetal HSC.

It is likely that the importance of this higher ontogeny-related susceptibility extend to the other human megakaryocyte/platelet-related diseases (e.g., Trisomy 21 AMKL and thrombocytopenia absent radii syndrome)(53–55) but also to other pediatric leukemia, including lymphoid leukemia with MLL-AF4 (56), which prevalence peaks during childhood. Furthermore, multiple pediatric cancers are driven by strong epigenetic fusion oncogenes in the context of a low mutational burden, including Ewing's sarcoma and rhabdomyosarcoma, for which the cellular origin is poorly defined (13), and glioblastoma, for which oncogenic drivers have been recently shown to arise in stem cells (57). Therefore, a precise characterization of the changes in the cellular architecture of the relevant tissues of origin should improve our understanding of the heterogeneous clinical presentations in other pediatric cancers and facilitate the establishment of other disease models that may serve as experimental platforms to develop more selective therapeutic strategies.

AUTHORS CONTRIBUTION

Conception and design:

CKL, JS, TM

Development of methodology:

CKL, EN, ER, VS, SJK, MD, ND, CL, BG, FP

Acquisition of data (provided animals, acquired and managed patients, provided facilities, etc.):

CKL, EN, VS, ER, ZA, PB, CBN, FB, CT, YL, HL, ED, RM, FL, AP, SJK, LB, JLV, ED, WV, MG, RM, FL, AHFMP, SM, CN, IG, OAB, BG, AP, FP, JS

Analysis and interpretation of data (e.g., statistical analysis, biostatistics, computational analysis):
CKL, EN, ER, PB, CBN, EB, SM, ND, CL, IG, OAB, BG, AP, FP, JS, TM

Writing, review, and/or revision of the manuscript:
All authors

Study supervision:
JS, TM

ACKNOWLEDGMENTS

We are grateful to Michael Kyba for the generous gift of the *A2Lox-Cre* ES cells and to Peter D. Aplan and Olivier Delattre for critical reading of the manuscript. We thank Clarisse Thiollier, Olivier Bluteau, Lou Le Mouël, Claude Preudhomme, Lila Diamanti, Nassera Abermil, Julie Chaumeil and Sabine Juge for their expertise and helpful discussions. We thank the FMI transgenic core facility (J.F. Spetz and P. Kopp) for their help in establishing iETO2-GLIS2 transgenic mice, Gustave Roussy institute facilities for mouse care (Patrick Gonin and Karine Ser-Leroux), bioinformatics support (Philippe Dessen and Daniel Gautheret), and Paul Zanardo for excellent administrative assistance.

This work was supported by the Association Laurette Fugain (ALF-2015/13 to TM), SIRIC-SOCRATE (INCa-DGOS-INSERM 6043 to TM), Fondation pour la Recherche Médicale (to ZA: FRM-ING20150532273, CKL), Fondation de France (FdF-00057925 to CT and TM), Lady Tata Foundation (R14120LL to CT), Cancéropôle Ile de France (to CKL and Emergence 2015), Gustave Roussy Genomic Core Facility – TA2016 (to CKL), Institut National Du Cancer (PLBIO-2014-176 and PLBIO-2018-169 to TM), PAIR-Pédiatrie/CONECT-AML (COllaborative Network for Children and Teenagers with Acute Myeloblastic Leukemia: INCa-ARC-LIGUE_11905 and Association Laurette Fugain), Associazione Italiana Ricerca sul Cancro (to FL). AHFMP was supported by the Novartis Research Foundation. SJK and BG were supported by a Bloodwise Specialist Programme grant (12029) and infrastructure funding from the Wellcome to the Wellcome & MRC Cambridge Stem Cell Institute. JS was supported by the Swiss National Science Foundation (31003A_173224/1), the Swiss Cancer League (KFS-3487-08-2014), the San Salvatore Foundation (Lugano, Switzerland), the Novartis Foundation for Biomedical Research and the Gertrude von Meissner Foundation (Basel, Switzerland). TM is an Equipe Labellisée LIGUE principal investigator.

The authors declare no competing financial interests.

METHODS

Reagents and resources

Table S10 contains an extensive list of the relevant reagents.

Patient-derived data and material

Patient blood and BM samples were obtained with the informed consent of the patient or their family in accordance with national ethics law. Samples were subjected to Ficoll gradient, immunophenotyped, and used fresh or frozen in fetal bovine serum (FBS) supplemented with 10% DMSO for subsequent use. DNA and RNA were obtained from the mononuclear cell fractions using the manufacturer's recommendations (Qiagen). cDNA from 284 patients were available to detect the EG fusion via RT-PCR. The primer sequences are provided in Table S11.

Clinical data were obtained from the ELAM02 protocol. The present study focused on 385 of 438 children treated in the ELAM02 trial (Treating Patients with Childhood Acute Myeloid Leukemia with Interleukin-2; ClinicalTrials.gov NCT00149162)(37). Patient selection was based on the availability of genomic DNA and RNA upon AML diagnosis. Children aged 0 to 18 years newly diagnosed with AML were enrolled between March 2005 and December 2011. Patients diagnosed with acute promyelocytic leukemia, therapy-related AML or Down syndromes were excluded from the ELAM02 trial. The study was approved by the Ethics Committee of Saint-Antoine Paris University Hospital (Assistance Publique-Hôpitaux de Paris) and by the Institutional Review Board of the French Regulatory Agency. The study was conducted in accordance with the declaration of Helsinki. Data concerning age at diagnosis was also collected from the ELAM02 protocol and (9) including 87 AMKL patients.

Patient-Derived Xenotransplantation (PDX)

Patient-derived xenograft protocols have been described previously (8).

FISH

The DNA probe set obtained from Empire genomics (CBFA2T3 and GLIS2 FISH probes, AmpliTech, Compiègne, France) hybridizes to chromosome 16p13.3 at CBFA2T3 locus (Red) and 16q24.3 at GLIS2 (green) in normal metaphase spreads or interphase nuclei. FISH analysis was performed following the manufacturer's protocol. Interphase nuclei and metaphases were scored on Imager Z2 fluorescence microscope (Zeiss, France) using Isis/Metafer/Relosys MetaSystems Software (MetaSystems, Altlussheim GmbH, Germany). In cells with the EG fusion, the overlap between the two probes generates a yellow signal indicative of the fusion oncogene.

Cell lines

The human AMKL MO7e cells (58) (derived from a 6-month-old girl) were cultured in MEM-α supplemented with 20% FBS, Penicillin (100U/mL)-Streptomycin (100µg/mL), 2mM L-Glutamine (Gibco) and 5 ng/ml of human GM-CSF (PeproTech).

The human CMS cells (59) (derived from a 2-years-old girl) were cultured in RPMI1640 supplemented with 10% FBS, Penicillin (100U/mL)-Streptomycin (100µg/mL), and 2mM L-Glutamine (Gibco).

The human AML-M6 HEL 92.1.7 (HEL) cells (60) (derived from a 30-years-old patient) were cultured in RPMI1640 supplemented with 10% FBS, Penicillin (100U/mL)-Streptomycin (100µg/mL), and 2mM L-Glutamine (Gibco).

All cell lines were obtained from the laboratory of O. Bernard in 2009, were karyotyped for authentication in 2018, were tested for mycoplasma in 2017 and the described experiments were performed within 3 months after thawing.

Mice

To generate the *iETO2-GLIS2:rtTA* (iEG) model, the human *EG* cDNA was cloned into the *p2Lox* vector and electroporated into A2Lox-Cre embryonic stem (ES) cells, a generous gift

from Michael Kyba (61). ES cell clones were selected for the correct integration of EG at the *Hprt* locus on chromosome X and used to obtain germline-transmitting chimeras that were subsequently backcrossed into the C57BL/6 background. Genotyping of the reverse tetracycline-controlled transactivator (rtTA) and the *EG* transgene were genotyped using the primers indicated in Table S11.
To obtain GFP^+-expressing iEG mice and track the iEG cells upon *in vivo* transplantations, we crossed *iETO2-GLIS2:rtTA* with the *Ubiquitin-GFP* reporter line (UBI-GFP) mice (62). In these mice, GFP expression is controlled by an ubiquitous promoter and not controlled by Dox. Therefore, engraftment of all CTRL and iEG donor cells can be tracked using GFP regardless of the Dox treatment status or iEG expression.
The transgenic mouse line for inducible expression of MLL-AF9 has been described previously (25).
The *iETO2-GLIS2* and *iMLL-AF9* transgenes were induced with doxycycline provided in impregnated food pellets (Dox food pellets, 545 mg/kg, Provider: SSNIF), which is predicted to correspond to an approximate dose of 2.2 mg/day.
Mice were maintained at the Gustave Roussy preclinical facility and all experiments were approved by the French National Animal Care and Use Committee (CEEA 26: #2012-017, #201712180922196_v2 and #2017122111548235_v2).

Bone Marrow Transplantation
Transplantation of bone marrow (BM, 10^6) or sorted progenitor cells were performed through intravenous injection in lethally (9.5 Gy) or sub-lethally (5Gy) irradiated 8-week-old C57BL/6 recipient mice.
Morphologic analysis of peripheral blood, BM, and spleen cells as well as histological analyses were performed according to standard procedures.

Flow Cytometry
Cells analyzed by flow cytometry were antibody stained in PBS 1X supplemented with 2% FBS for 30 minutes at 4°C with washing prior to FACS analysis. Whole BM and spleen cells from mice were collected, subjected to RBC lysis and stained for FACS analysis.
To obtain hematopoietic stem and progenitor cells (HSPC), BM cells were depleted from the mature hematopoietic cells (Lin^-) with the Becton Dickinson (BD) Mouse Hematopoietic Progenitor (stem) Cell enrichment Set (558451).
To obtain adult BM (ABM) precise progenitors populations were further purified by FACS according to the following phenotypes: LT-HSC (HSC) were defined as $LIN^-Kit^+Sca1^+CD135^-CD34^-CD48^-CD150^+$, MPP2 cells were defined as $LIN^-Kit^+Sca1^+CD135^-CD34^+CD48^+CD150^+$, MPP3 cells were defined as $LIN^-Kit^+Sca1^+CD135^-CD34^+CD48^+CD150^-$, and MPP4 cells were defined as $LIN^-Kit^+Sca1^+CD135^+CD34^+CD48^+CD150^-$.
To obtain fetal liver HSPC, cells were depleted with Biotin-conjugated antibodies against CD3, Ter119, B220, Gr1, NK1.1, F4/80, CD19.
To obtain FL HSC and progenitor populations, cells were purified by FACS according to the following phenotypes: LT-HSC were defined as LIN-Kit+Sca1+CD135-CD48-CD150+, while MPP2, MPP3 and MPP4 cells were defined with the same markers as ABM cells.
Flow cytometry analyses were performed with an ARIAII, ARIAIII, CANTO-II or CANTO-X instruments (BD), and data were analyzed using FlowJo software (version Flowjo 9.3.2).

Serial replating assays
Total cells and/or progenitors from ABM or FL at E12.5 or E14.5 were isolated from iEG mice and plated in 3mL methylcellulose (Methocult M3434; StemCell Technologies, Canada), supplemented with IL3, IL6, SCF, EPO and 300ng/ml DOX. Colonies were scored under the microscope after five to seven days, harvested and replated (10^4 cells) for four rounds.

Single cell cultures
Single cells were seeded in 96-well plates in 100ul RPMI supplemented with 10% FBS, cytokines (mIL3, mIL6, mIL11, mSCF, mTPO, mEPO, mGM-CSF, mFLT3l) and 100ng/ml Dox.

Wells were scored for clonal growth after four days of culture and frequency of megakaryoblastic and myeloid cells was assessed by surface marker analysis using a previously described method (63) after five to ten days.

RNA extraction & quantitative RT-PCR analysis

mRNA was isolated using an RNeasy Mini/Micro kit (Qiagen) and quantified using a NanoDrop (ThermoScientific). Reverse transcription was carried out with SuperScript II (Invitrogen). Q-PCR was performed with SYBR Select Master Mix or Taqman Gene Expression Master Mix (Applied Biosystems) using a 7500HT Fast Real-Time PCR System (Applied Biosystems) according to the manufacturer's recommendations. The primer sequences are provided in Table S11.

ETO2-GLIS2 genomic DNA fusion point

DNA were isolated using an All Prep DNA/RNA Mini/Micro kit (Qiagen) and quantified using a NanoDrop (ThermoScientific). PCR was performed using a GeneAmp PCR System 9700. The primer sequences are provided in Table S11.

Immunoblotting

Total cell lysates were prepared in lysate buffer containing 50 mM Tris-HCl (pH 8), 150 mM NaCl, 1% NP40, 1 mM EDTA, 0.1% SDS, 0.5% DOC, and protease inhibitors (PMSF 1X, NAF 1X, Sodium orthovanadate 1X, complete 1X). Western blotting was then performed using standard procedures using anti-ETO2 (ab33072, Abcam), anti-HSC70 (sc7298, Santa Cruz Biotechnology) and anti-RPLP0 (ab192866, Abcam) antibodies.

Production of retroviral particles and transduction

For retroviral transduction experiments, we constructed murine stem cell virus (MSCV) backbone constructs expressing GFP and encoding human *ETO2-GLIS2*, *ERG, CEBPA, SPI1, GATA1* ORF. Briefly, 293T cells were transfected using Xtreme GENE transfection reagent according to the manufacturer's instructions (Roche). Retroviral particles were harvested 24 and 48 hours after transfection. For retroviral transduction, murine progenitor cells were spinoculated twice with retroviral particles in culture media containing 5 µg/mL polybrene and 7.5 mM HEPES buffer for 90 minutes at 2500 rpm and 33°C.

Single cell RNAseq (scRNAseq)

Progenitor cells were isolated from iEG mice and cultured for 24 hours in RPMI supplemented with 10% FBS, cytokines (mIL3, mIL6, mSCF, mTPO, mFLT3l) and 100 ng/ml Dox. ScRNAseq analysis was performed as described previously (28,64). Single cells were individually sorted in 96-well plates containing lysis buffer (0.2% Triton X-100 and 500U/ml Superase-In RNase Inhibitor). The Illumina Nextera XT DNA preparation kit was used to prepare libraries. Pooled libraries were sequenced using the Illumina Hisequation 4000 system (single-end 125 base pair reads).

Statistical analyses

Statistical analyses were performed using the GraphPad Prism software (version Prism 6-2) except otherwise mentioned.

Bioinformatics analyses

Reads quality control and alignment: Quality control of reads was performed using FastQC 0.11.7 and multiQC 1.5.dev0. The reads were aligned to the reference genome mm10 GRCm38.p4 81 with GSNAP (v 2015-09-29) with the following parameters: -A sam -B 5 -t 23 -n 1 -Q -N 1. Finally, gene expression was quantified using HTSeq 0.6.0

Counts pre-processing, quality controls and normalization: prior to data normalization, cells were filtered to remove low quality samples and to fulfil the following conditions: have at least 4000 detectable genes, have less than 20% of counts mapping to mitochondrial genes, have less than 50% of reads mapping to spike in controls and at least 2^5 counts that map to nuclear

genes. Normalization was next performed by library size with the deconvolution of size factors method described by Lun et al. using *scran* and *scater* R libraries (65,66). Pre-clustering of cells and five pool sizes from 20 to 100 (by an increment of 20) were used as normalization parameters. High variable genes (HVG) selection was performed as previously described (67) for feature selection. Those HVG were used for t-SNE to explore possible underlying substructures in the data.

Differential expression analysis and gene set enrichment analysis (GSEA): for detection of differences at the transcriptomic level between groups, differential expression analysis was performed with Wilcoxon test over the log2 counts values and p-value correction by Benjamini-Hochenberg (FDR cut-off at 0.05). GSEA was also performed to detect potential overexpressed signatures in patients with default parameters except for –collapse false –permute phenotype (68).

Gene Regulatory Network inference: ARACNe-AP software was used to infer a Gene Regulatory Network (69) using iEG scRNAseq data to predicted a list of target genes of each TF in the context of cells expressing ETO2-GLIS2 (called "EG network", Table S6). For that purpose, iEG cells with log2 counts < 1 for ETO2-GLIS2 were not considered. ARACNe was ran over the log2 normalized counts in bootstrap mode (100 iterations), with a p-value threshold of 1e-8 and a custom curated list of 2171 TFs. Similarly, we predicted the target genes of each TF in a normal hematopoietic context from published scRNAseq data (70) obtained with the same protocol (called "normal network", Table S7). Therefore, the activity of each TF was computed using two independent lists of target genes and consistent prediction of TF activity levels were obtained for key factors (Figure 5E).

Transcription regulator activity prediction and Master Regulator Analysis: networks were used to infer activity (Normalized Enrichment Score, NES) of the transcriptomic regulator with R library *viper* (71), as described in the package manual. NES were used to test differential activity by t-test and p-value correction by Benjamini-Hochenberg (FDR cut-off at 0.05). Master Regulator Analysis was also carried out as described in the manual, with calculation of bootstrapped null model and shadow correction (enrichment of a regulator driven by similar targets of another regulator) of top 25 regulators.

ATACseq

ATACseq analysis has been adapted from (Buenrostro JD, 2015). Briefly, cells were isolated from iEG mice and cultured for 24 hours in RPMI supplemented with 10% FBS, cytokines (mIL3, mIL6, mSCF, mTPO, mFLT3l) and 100 ng/ml Dox. After cell lysis, transposition and purification step, the transposed DNA fragments were amplified by polymerase chain reaction (PCR) between 12 and 18 depending on the number of cells at the beginning (50,000 to 6,000) using adapters from the Nextera index kit (illumina). PCR purification was performed using Agencourt AMPure XP magnetic beads (Beckman Coulter A63880) in order to remove large fragments and remaining primers. Library quality was assessed using an Agilent 2100 Bioanalyzer using a High Sensitivity DNA chip (Agilent Technologies 5067-4626). Libraries were sequenced using Novaseq-6000 sequencer (Illumina) (50bp paired-end reads).

Quality control of reads was performed using FastQC 0.11.7 and multiQC 1.5. The reads were aligned to the reference genome mm10 with bwa (aln 0.7.17). After alignment, we removed reads mapping to the mitochondrial genome, PCR duplicate reads and reads with a mapping quality lower than 20 using samtools (v 1.9). Final read counts for all mouse datasets ranged from 37 to 128 million reads. Mapped reads were normalized to bins per million (BPM) and were converted to bigwig format using deeptools (v3.2.0). Peak calling, differential analysis, annotation and motif analysis was performed using macs2 (V 2.1.2), Diffbind R package (v 2.8.0 in R-3.5.1 with threshold log2(1.5)), and homer (v4.10.4, annotatePeak.pl and findMotifsGenome.pl) respectively.

Data availability

Single cell RNAseq data were deposited into EBI - Array-Express under the accession number E-MTAB-7213.

REFERENCES

1. Gröbner SN, Worst BC, Weischenfeldt J, Buchhalter I, Kleinheinz K, Rudneva VA, et al. The landscape of genomic alterations across childhood cancers. Nature. 2018;555:321–7.
2. Bolouri H, Farrar JE, Triche T, Ries RE, Lim EL, Alonzo TA, et al. The molecular landscape of pediatric acute myeloid leukemia reveals recurrent structural alterations and age-specific mutational interactions. Nat Med. 2018;24:103–12.
3. Greaves M. In utero origins of childhood leukaemia. Early Hum Dev. 2005;81:123–9.
4. Hong D, Gupta R, Ancliff P, Atzberger A, Brown J, Soneji S, et al. Initiating and cancer-propagating cells in TEL-AML1-associated childhood leukemia. Science. 2008;319:336–9.
5. Slany RK. The molecular biology of mixed lineage leukemia. Haematologica. 2009;94:984–93.
6. Sanjuan-Pla A, Bueno C, Prieto C, Acha P, Stam RW, Marschalek R, et al. Revisiting the biology of infant t(4;11)/MLL-AF4+ B-cell acute lymphoblastic leukemia. Blood. 2015;126:2676–85.
7. Creutzig U, Büchner T, Sauerland MC, Zimmermann M, Reinhardt D, Döhner H, et al. Significance of age in acute myeloid leukemia patients younger than 30 years: a common analysis of the pediatric trials AML-BFM 93/98 and the adult trials AMLCG 92/99 and AMLSG HD93/98A. Cancer. 2008;112:562–71.
8. Thiollier C, Lopez CK, Gerby B, Ignacimouttou C, Poglio S, Duffourd Y, et al. Characterization of novel genomic alterations and therapeutic approaches using acute megakaryoblastic leukemia xenograft models. J Exp Med. 2012;209:2017–31.
9. de Rooij JDE, Branstetter C, Ma J, Li Y, Walsh MP, Cheng J, et al. Pediatric non-Down syndrome acute megakaryoblastic leukemia is characterized by distinct genomic subsets with varying outcomes. Nat Genet. 2017;49:451–6.
10. Lopez CK, Malinge S, Gaudry M, Bernard OA, Mercher T. Pediatric Acute Megakaryoblastic Leukemia: Multitasking Fusion Proteins and Oncogenic Cooperations. Trends Cancer. 2017;3:631–42.
11. Gough SM, Slape CI, Aplan PD. NUP98 gene fusions and hematopoietic malignancies: common themes and new biologic insights. Blood. 2011;118:6247–57.
12. Masetti R, Pigazzi M, Togni M, Astolfi A, Indio V, Manara E, et al. CBFA2T3-GLIS2 fusion transcript is a novel common feature in pediatric, cytogenetically normal AML, not restricted to FAB M7 subtype. Blood. 2013;121:3469–72.
13. Grünewald TGP, Cidre-Aranaz F, Surdez D, Tomazou EM, de Álava E, Kovar H, et al. Ewing sarcoma. Nat Rev Dis Primer. 2018;4:5.
14. Bardini M, Spinelli R, Bungaro S, Mangano E, Corral L, Cifola I, et al. DNA copy-number abnormalities do not occur in infant ALL with t(4;11)/MLL-AF4. Leukemia. 2010;24:169–76.
15. Krivtsov AV, Feng Z, Lemieux ME, Faber J, Vempati S, Sinha AU, et al. H3K79 methylation profiles define murine and human MLL-AF4 leukemias. Cancer Cell. 2008;14:355–68.
16. Thirant C, Ignacimouttou C, Lopez CK, Diop M, Le Mouël L, Thiollier C, et al. ETO2-GLIS2 Hijacks Transcriptional Complexes to Drive Cellular Identity and Self-Renewal in Pediatric Acute Megakaryoblastic Leukemia. Cancer Cell. 2017;31:452–65.
17. Dawson MA, Prinjha RK, Dittmann A, Giotopoulos G, Bantscheff M, Chan W-I, et al. Inhibition of BET recruitment to chromatin as an effective treatment for MLL-fusion leukaemia. Nature. 2011;478:529–33.
18. Erb MA, Scott TG, Li BE, Xie H, Paulk J, Seo H-S, et al. Transcription control by the ENL YEATS domain in acute leukaemia. Nature. 2017;543:270–4.
19. Babovic S, Eaves CJ. Hierarchical organization of fetal and adult hematopoietic stem cells. Exp Cell Res. 2014;329:185–91.
20. Elagib KE, Brock AT, Goldfarb AN. Megakaryocyte ontogeny: Clinical and molecular significance. Exp Hematol. 2018;61:1–9.

21. Laurenti E, Göttgens B. From haematopoietic stem cells to complex differentiation landscapes. Nature. 2018;553:418–26.
22. Sanjuan-Pla A, Macaulay IC, Jensen CT, Woll PS, Luis TC, Mead A, et al. Platelet-biased stem cells reside at the apex of the haematopoietic stem-cell hierarchy. Nature. 2013;502:232–6.
23. Carrelha J, Meng Y, Kettyle LM, Luis TC, Norfo R, Alcolea V, et al. Hierarchically related lineage-restricted fates of multipotent haematopoietic stem cells. Nature. 2018;554:106–11.
24. Rodriguez-Fraticelli AE, Wolock SL, Weinreb CS, Panero R, Patel SH, Jankovic M, et al. Clonal analysis of lineage fate in native haematopoiesis. Nature. 2018;553:212–6.
25. Stavropoulou V, Kaspar S, Brault L, Sanders MA, Juge S, Morettini S, et al. MLL-AF9 Expression in Hematopoietic Stem Cells Drives a Highly Invasive AML Expressing EMT-Related Genes Linked to Poor Outcome. Cancer Cell. 2016;30:43–58.
26. Notta F, Zandi S, Takayama N, Dobson S, Gan OI, Wilson G, et al. Distinct routes of lineage development reshape the human blood hierarchy across ontogeny. Science. 2016;351:aab2116.
27. Paul F, Arkin Y, Giladi A, Jaitin DA, Kenigsberg E, Keren-Shaul H, et al. Transcriptional Heterogeneity and Lineage Commitment in Myeloid Progenitors. Cell. 2015;163:1663–77.
28. Wilson NK, Kent DG, Buettner F, Shehata M, Macaulay IC, Calero-Nieto FJ, et al. Combined Single-Cell Functional and Gene Expression Analysis Resolves Heterogeneity within Stem Cell Populations. Cell Stem Cell. 2015;16:712–24.
29. Velten L, Haas SF, Raffel S, Blaszkiewicz S, Islam S, Hennig BP, et al. Human haematopoietic stem cell lineage commitment is a continuous process. Nat Cell Biol. 2017;19:271–81.
30. Yuan J, Nguyen CK, Liu X, Kanellopoulou C, Muljo SA. Lin28b reprograms adult bone marrow hematopoietic progenitors to mediate fetal-like lymphopoiesis. Science. 2012;335:1195–200.
31. Copley MR, Babovic S, Benz C, Knapp DJHF, Beer PA, Kent DG, et al. The Lin28b-let-7-Hmga2 axis determines the higher self-renewal potential of fetal haematopoietic stem cells. Nat Cell Biol. 2013;15:916–25.
32. Bluteau O, Langlois T, Rivera-Munoz P, Favale F, Rameau P, Meurice G, et al. Developmental changes in human megakaryopoiesis. J Thromb Haemost JTH. 2013;11:1730–41.
33. Rowe RG, Wang LD, Coma S, Han A, Mathieu R, Pearson DS, et al. Developmental regulation of myeloerythroid progenitor function by the Lin28b-let-7-Hmga2 axis. J Exp Med. 2016;213:1497–512.
34. Xu J, Shao Z, Li D, Xie H, Kim W, Huang J, et al. Developmental control of polycomb subunit composition by GATA factors mediates a switch to non-canonical functions. Mol Cell. 2015;57:304–16.
35. Ye M, Zhang H, Amabile G, Yang H, Staber PB, Zhang P, et al. C/EBPa controls acquisition and maintenance of adult haematopoietic stem cell quiescence. Nat Cell Biol. 2013;15:385–94.
36. Pimkin M, Kossenkov AV, Mishra T, Morrissey CS, Wu W, Keller CA, et al. Divergent functions of hematopoietic transcription factors in lineage priming and differentiation during erythro-megakaryopoiesis. Genome Res. 2014;24:1932–44.
37. Petit A, Ducassou S, Leblanc T, Pasquet M, Rousseau A, Ragu C, et al. Maintenance Therapy With Interleukin-2 for Childhood AML: Results of ELAM02 Phase III Randomized Trial. HemaSphere. 2018;2:e159.
38. Cabezas-Wallscheid N, Klimmeck D, Hansson J, Lipka DB, Reyes A, Wang Q, et al. Identification of regulatory networks in HSCs and their immediate progeny via integrated proteome, transcriptome, and DNA methylome analysis. Cell Stem Cell. 2014;15:507–22.

39. Chen W, Kumar AR, Hudson WA, Li Q, Wu B, Staggs RA, et al. Malignant transformation initiated by Mll-AF9: gene dosage and critical target cells. Cancer Cell. 2008;13:432–40.
40. Bourquin J-P, Subramanian A, Langebrake C, Reinhardt D, Bernard O, Ballerini P, et al. Identification of distinct molecular phenotypes in acute megakaryoblastic leukemia by gene expression profiling. Proc Natl Acad Sci U S A. 2006;103:3339–44.
41. Gruber TA, Larson Gedman A, Zhang J, Koss CS, Marada S, Ta HQ, et al. An Inv(16)(p13.3q24.3)-encoded CBFA2T3-GLIS2 fusion protein defines an aggressive subtype of pediatric acute megakaryoblastic leukemia. Cancer Cell. 2012;22:683–97.
42. Giladi A, Paul F, Herzog Y, Lubling Y, Weiner A, Yofe I, et al. Single-cell characterization of haematopoietic progenitors and their trajectories in homeostasis and perturbed haematopoiesis. Nat Cell Biol. 2018;20:836–46.
43. Hoppe PS, Schwarzfischer M, Loeffler D, Kokkaliaris KD, Hilsenbeck O, Moritz N, et al. Early myeloid lineage choice is not initiated by random PU.1 to GATA1 protein ratios. Nature. 2016;535:299–302.
44. Bresnick EH, Lee H-Y, Fujiwara T, Johnson KD, Keles S. GATA switches as developmental drivers. J Biol Chem. 2010;285:31087–93.
45. Dang J, Nance S, Ma J, Cheng J, Walsh MP, Vogel P, et al. AMKL chimeric transcription factors are potent inducers of leukemia. Leukemia. 2017;31:2228–34.
46. Takano H, Ema H, Sudo K, Nakauchi H. Asymmetric division and lineage commitment at the level of hematopoietic stem cells: inference from differentiation in daughter cell and granddaughter cell pairs. J Exp Med. 2004;199:295–302.
47. Haas S, Hansson J, Klimmeck D, Loeffler D, Velten L, Uckelmann H, et al. Inflammation-Induced Emergency Megakaryopoiesis Driven by Hematopoietic Stem Cell-like Megakaryocyte Progenitors. Cell Stem Cell. 2015;17:422–34.
48. Niu C, Zhang J, Breslin P, Onciu M, Ma Z, Morris SW. c-Myc is a target of RNA-binding motif protein 15 in the regulation of adult hematopoietic stem cell and megakaryocyte development. Blood. 2009;114:2087–96.
49. Knudsen KJ, Rehn M, Hasemann MS, Rapin N, Bagger FO, Ohlsson E, et al. ERG promotes the maintenance of hematopoietic stem cells by restricting their differentiation. Genes Dev. 2015;29:1915–29.
50. Rosenbauer F, Wagner K, Kutok JL, Iwasaki H, Le Beau MM, Okuno Y, et al. Acute myeloid leukemia induced by graded reduction of a lineage-specific transcription factor, PU.1. Nat Genet. 2004;36:624–30.
51. Carmichael CL, Metcalf D, Henley KJ, Kruse EA, Di Rago L, Mifsud S, et al. Hematopoietic overexpression of the transcription factor Erg induces lymphoid and erythro-megakaryocytic leukemia. Proc Natl Acad Sci U S A. 2012;109:15437–42.
52. Zhang P, Iwasaki-Arai J, Iwasaki H, Fenyus ML, Dayaram T, Owens BM, et al. Enhancement of hematopoietic stem cell repopulating capacity and self-renewal in the absence of the transcription factor C/EBP alpha. Immunity. 2004;21:853–63.
53. Roberts I, Izraeli S. Haematopoietic development and leukaemia in Down syndrome. Br J Haematol. 2014;167:587–99.
54. Albers CA, Newbury-Ecob R, Ouwehand WH, Ghevaert C. New insights into the genetic basis of TAR (thrombocytopenia-absent radii) syndrome. Curr Opin Genet Dev. 2013;23:316–23.
55. Liu Z-J, Sola-Visner M. Neonatal and adult megakaryopoiesis. Curr Opin Hematol. 2011;18:330–7.
56. Barrett NA, Malouf C, Kapeni C, Bacon WA, Giotopoulos G, Jacobsen SEW, et al. Mll-AF4 Confers Enhanced Self-Renewal and Lymphoid Potential during a Restricted Window in Development. Cell Rep. 2016;16:1039–54.
57. Lee JH, Lee JE, Kahng JY, Kim SH, Park JS, Yoon SJ, et al. Human glioblastoma arises from subventricular zone cells with low-level driver mutations. Nature. 2018;560:243–7.
58. Avanzi GC, Lista P, Giovinazzo B, Miniero R, Saglio G, Benetton G, et al. Selective growth response to IL-3 of a human leukaemic cell line with megakaryoblastic features. Br J Haematol. 1988;69:359–66.

59. Sato T, Sekine H, Kakuda H, Miura N, Sunohara M, Fuse A. HIV infection of megakaryocytic cell lines. Leuk Lymphoma. 2000;36:397–404.
60. Martin P, Papayannopoulou T. HEL cells: a new human erythroleukemia cell line with spontaneous and induced globin expression. Science. 1982;216:1233–5.
61. Iacovino M, Bosnakovski D, Fey H, Rux D, Bajwa G, Mahen E, et al. Inducible cassette exchange: a rapid and efficient system enabling conditional gene expression in embryonic stem and primary cells. Stem Cells Dayt Ohio. 2011;29:1580–8.
62. Schaefer BC, Schaefer ML, Kappler JW, Marrack P, Kedl RM. Observation of antigen-dependent CD8+ T-cell/ dendritic cell interactions in vivo. Cell Immunol. 2001;214:110–22.
63. Månsson R, Hultquist A, Luc S, Yang L, Anderson K, Kharazi S, et al. Molecular evidence for hierarchical transcriptional lineage priming in fetal and adult stem cells and multipotent progenitors. Immunity. 2007;26:407–19.
64. Picelli S, Faridani OR, Björklund AK, Winberg G, Sagasser S, Sandberg R. Full-length RNA-seq from single cells using Smart-seq2. Nat Protoc. 2014;9:171–81.
65. Yip SH, Sham PC, Wang J. Evaluation of tools for highly variable gene discovery from single-cell RNA-seq data. Brief Bioinform. 2018;
66. Lun ATL, Bach K, Marioni JC. Pooling across cells to normalize single-cell RNA sequencing data with many zero counts. Genome Biol. 2016;17:75.
67. Brennecke P, Anders S, Kim JK, Kołodziejczyk AA, Zhang X, Proserpio V, et al. Accounting for technical noise in single-cell RNA-seq experiments. Nat Methods. 2013;10:1093–5.
68. Subramanian A, Tamayo P, Mootha VK, Mukherjee S, Ebert BL, Gillette MA, et al. Gene set enrichment analysis: a knowledge-based approach for interpreting genome-wide expression profiles. Proc Natl Acad Sci U S A. 2005;102:15545–50.
69. Lachmann A, Giorgi FM, Lopez G, Califano A. ARACNe-AP: gene network reverse engineering through adaptive partitioning inference of mutual information. Bioinforma Oxf Engl. 2016;32:2233–5.
70. Nestorowa S, Hamey FK, Pijuan Sala B, Diamanti E, Shepherd M, Laurenti E, et al. A single-cell resolution map of mouse hematopoietic stem and progenitor cell differentiation. Blood. 2016;128:e20-31.
71. Alvarez MJ, Shen Y, Giorgi FM, Lachmann A, Ding BB, Ye BH, et al. Functional characterization of somatic mutations in cancer using network-based inference of protein activity. Nat Genet. 2016;48:838–47.
72. van Zutven LJCM, Onen E, Velthuizen SCJM, van Drunen E, von Bergh ARM, van den Heuvel-Eibrink MM, et al. Identification of NUP98 abnormalities in acute leukemia: JARID1A (12p13) as a new partner gene. Genes Chromosomes Cancer. 2006;45:437–46.
73. Struski S, Lagarde S, Bories P, Puiseux C, Prade N, Cuccuini W, et al. NUP98 is rearranged in 3.8% of pediatric AML forming a clinical and molecular homogenous group with a poor prognosis. Leukemia. 2017;31:565–72.
74. Hara Y, Shiba N, Ohki K, Tabuchi K, Yamato G, Park M-J, et al. Prognostic impact of specific molecular profiles in pediatric acute megakaryoblastic leukemia in non-Down syndrome. Genes Chromosomes Cancer. 2017;56:394–404.
75. de Rooij JDE, Hollink IHIM, Arentsen-Peters STCJM, van Galen JF, Berna Beverloo H, Baruchel A, et al. NUP98/JARID1A is a novel recurrent abnormality in pediatric acute megakaryoblastic leukemia with a distinct HOX gene expression pattern. Leukemia. 2013;27:2280–8.
76. Aran D, Hu Z, Butte AJ. xCell: digitally portraying the tissue cellular heterogeneity landscape. Genome Biol. 2017;18:220.

FIGURE LEGENDS

Figure 1.
AMKL is diagnosed at a younger age than AML in pediatric patients.

A, Representative fluorescent in situ hybridization with probes detecting *ETO2* (Green) and *GLIS2* (Red) in leukemic cells from an EG^+ AML patient. The yellow signal results from the red-green overlap, thus indicating the derivative chromosome carrying the EG fusion.
B, Frequencies of EG^+ patients with AMKL (n=34), other AML subtypes ("AML M0-5", n=242) and in the entire ELAM02 cohort ("All AML", n= 276).
C, Age at diagnosis of EG^+ patients obtained from pooling data from the ELAM02 cohort and published reports (9,12,72–75). AMKL (n=33) vs AML (n=15), p<0.0001.
D, Age at diagnosis of NUP98-$KDM5A^+$ patients, AMKL (n=27) vs AML (n=4), p=0.0017.
E, Age at diagnosis of patients with MLL fusions, AMKL (n=18) vs AML (n=88), p=0.095.
F, Age at diagnosis of patients with AMKL (n=132) vs. other AML (n=500) subtypes, p<0.0001.
G, Flow cytometry analyses of primary patient-derived xenografts (PDX) obtained from AMKL and AML patients. Analyses are gated on $CD34^+$ human blasts.
H, Experimental design of flow cytometric sorting of the three blast populations analyzed in (I-K).
I, Representative cell morphology of the three leukemic cell populations on cytospots. Wright-Giemsa staining. Magnification: x100.
J, Secondary xenotransplantation of various cell populations from patient #5 indicates that only $CD41^-CD15^-$ cells propagated the disease.
K, CD15 and CD41 expression on $CD34^+$ cells obtained from recipients of $3x10^5$ $CD15^-CD41^-$ cells one-year post-transplant.
Statistical significance is indicated as p values (Student's t test). *: p<0.05, **: p<0.01, ***: p<0.001.

Figure 2.
ETO2-GLIS2 efficiently induces leukemia in mice.

A, Experimental design: disease-inducing potential was assessed by providing doxycycline (Dox) to naive iEG female mice (primary). Cell autonomous leukemogenesis was ascertained by transplanting 10^6 BM cells from iEG mice induced at eight weeks of age and for 45 days into wild-type C57BL/6 recipients with or without exposure to Dox (secondary).
B, Representative flow cytometry analysis of Kit^+ and $CD41^+$ expression (upper panels) or $CD11b^+$ and $Gr1^+$ expression (lower panels) in Bone Marrow of primary diseased iEG mice defining 2 phenotypes: Group1=megakaryoblastic (primarily $CD41^+$) and Group2=immature/myeloid (heterogeneous expression of Kit^+ and $CD11b^+Gr1^+$ markers) (CTRL n=5, iEG n=19 in total).
C, Spleen histology of primary mice (CTRL, Group 1 and Group 2). Upper panels: Hematoxylin-Eosin-Safran staining, lower panels: VWF staining (brown coloration).
D, Kaplan-Meier survival plot of Dox-exposed iEG mice according to the two phenotypes described in (B) (CTRL n=11, iEG n=19 in total, CTRL vs. Group1: p=0.0001, CTRL vs. Group2: p<0.0001). Median survival: Group 1=164 days, Group2 = 251 days.
E, Spleen and liver weights in primary iEG mice according to the two phenotypes described in (B) (1 = $CD41^+$ and 2 = immature/$CD11b^+Gr1^+$). Spleen (CTRL vs. Group1: p=0.0002, CTRL vs. Group2: p=0.0023), liver (CTRL vs. Group1: p=0.0060, CTRL vs. Group2: p=0.0016).
F, Peripheral blood counts of diseased iEG mice with the different phenotypes. RBC (CTRL vs. Group1: p<0.0001, CTRL vs. Group2: p<0.0001), WBC (CTRL vs. Group1: p=0.0068, CTRL vs. Group2: p=0.7624), Platelet (Plt: CTRL vs. Group1: p=0.3902, CTRL vs. Group2: p=0.6533).
G, Kaplan-Meier survival plot of secondary recipients with or without Dox-exposure (Dox -: n=4, Dox +: n=6). p=0.0110 (Log rank Mantel-Cox test).
H, Representative spleen section of a secondary recipient stained with VWF (brown coloration) shows significant organ infiltration.

I, Spleen and liver weights in secondary recipients with or without Dox-exposure. Spleen: p=0.0025, liver: p=0.0220.
J, Quantification of flow cytometry analyses in the spleen of secondary recipients with or without Dox-exposure. Kit^+: p=0.0026, $CD41^+$: p=0.0015, $CD11b^+Gr1^+$: p=0.1002.
Statistical significance is indicated as p values (Student's t test except when otherwise specified). *: p<0.05, **: p<0.01, ***: p<0.001.

Figure 3.
Developmental stage determines the phenotype of ETO2-GLIS2$^+$ leukemia.
A, Experimental design to address the impact of EG on the clonogenic potential of fetal liver (FL) or adult bone marrow (ABM) progenitors in methylcellulose shown in (B) and (C) or *in vivo* shown in (D to H).
B, Number of colonies upon culture of 2,500 fetal liver (FL E12.5) or Lin^- BM cells at two weeks (newborn) or two months post-partum (ABM) in Dox-containing methylcellulose conditions. Serial replating was performed every seven days. P1: first plate, P2: secondary plate, P3: tertiary plate, P4: quaternary plate, P5: fifth plate. FL P5 p<0.0001, newborn P4 p=0.0034, ABM P4 p=0.0246.
C, Representative flow cytometry analysis of $CD41^+$ and $Gr1^+$ expression at P3 (upper panels) and percentages of $CD41^+$ and $Gr1^+$ cells at P1 to P3 (lower panels).
D, Kaplan-Meier survival plot of wild type Dox-treated recipients engrafted with $1x10^6$ ABM or FL cells from double transgenic iEG^+Ubiquitin-GFP^+ (GFP^+). Log rank Mantel-Cox test: p<0.0001. Median survival FL = 39 days, ABM = 397 days.
E, Spleen weights in CTRL and diseased mice at time of sacrifice (CTRL vs. FL: p=0.0005, CTRL vs. ABM: p=0.1999, FL vs. ABM p<0.0001).
F, Peripheral blood counts of recipients of FL and ABM. WBC (CTRL vs. FL: p=0.0037, CTRL vs. ABM: p=0.9125, FL vs. ABM p<0.0001), RBC (CTRL vs. FL: p=0.0004, CTRL vs. ABM: p=0.0041, FL vs. ABM p=0.0133), Platelets (Plt: CTRL vs. FL: p=0.0003, CTRL vs. ABM: p=0.0137, FL vs. ABM p=0.0181).
G, Representative flow cytometry analyses of BM cells from diseased recipients at time of sacrifice.
H, Quantification of GFP^+ (CTRL vs. FL: p=0.2644, CTRL vs. ABM: p<0.0001, FL vs. ABM p<0.0001), $CD41^+$ (CTRL vs. FL: p=0.0154, CTRL vs. ABM: p=0.1870, FL vs. ABM p<0.0001) and $CD11b^+Gr1^+$ (CTRL vs. FL: p=0.0024, CTRL vs. ABM: p=0.6335, FL vs. ABM p=0.0167) in GFP^+ BM cells.
I, Images of E14.5 embryos (left and middle panels) and corresponding FL (right panels) obtained from pregnant females on Dox for 36 hours.
J, Flow cytometry analyses of FL cells obtained in (I) (CTRL n=8, iEG n=10). $CD71^+Ter119^+$: p<0.0001, $CD11b^+Gr1^+$: p=0.0380, $CD41^+$: p<0.0001.
Statistical significance is indicated as p values (Student's t test except when otherwise specified). *: p<0.05, **: p<0.01, ***: p<0.001.

Figure 4.
ETO2-GLIS2-induced AMKL is an HSC-derived leukemia.
A, Experimental design to address the clonogenic potential of HSC and MPP from CTRL and iEG E14.5 embryos. Serial replating was performed every seven days for four weeks (P1 to P4).
B, Representative flow cytometry analyses of cells obtained from the first plate (P1).
C, Number of colonies upon serial replating. Mean+/-SEM is indicated.
D, Representative flow cytometry analyses of cells grown in methylcellulose cultures with and without Dox.
E, Experimental design to address the clonogenic potential of adult (8-10 weeks-old) HSC and MPP from iEG and CTRL mice.
F, Representative flow cytometry analyses of cells obtained at P1.

G, Number of colonies upon serial replating. Mean+/-SEM is indicated.
H, Wright-Giemsa stained cytospots from iEG ABM HSC- and MPP4-derived methylcellulose cultures at P3. Magnification: x100.
I, Single HSC and MPP3 ABM cells from CTRL or iEG mice were evaluated for their potential to develop myeloid ($Gr1^+$), megakaryoblastic ($CD41^+$) or mixed cell populations (containing both $Gr1^+CD41^-$ and $Gr1^-CD41^+$ cells) in 96-wells liquid cultures with Dox treatment. A representative flow cytometry analysis of the three types of colonies obtained after eight days of culture is shown.
J, Histogram representing the percentages of $CD41^+$, $Gr1^+$ or mixed population colonies as defined in (I), (HSC CTRL: n=50, HSC iEG: n=47, MPP3 CTRL: n=53 and MPP3 iEG: n=85).

Figure 5.
ETO2-GLIS2 alters the LT-HSC transcriptional network in an ontogeny-dependent manner
A, Clustering of the different populations based on scRNAseq data using Zinbwave. The number of genes significantly differentially expressed between CTRL vs. iEG in each population is indicated.
B, Gene Set Enrichment Analysis on iEG FL LT-HSC (left panel) or ABM LT-HSC (right panel) vs. CTRL scRNAseq data using published EG^+ AMKL patients' specific gene expression signatures from Bourquin et al. (40) or Gruber et al. (41). Enrichment score (NES) in iEG vs. CTRL are represented (positive NES indicates higher activity in iEG vs CTRL cells, negative NES indicates lower activity in iEG vs CTRL cells). Up: signature of genes upregulated in EG^+ AMKL patients, Down: signature of genes downregulated in EG^+ AMKL patients. *: FDR<0.25, **: FDR<0.05, ***: FDR<0.01.
C, GSEA using published signatures from normal progenitors and mature cells (38,76): HSC, MPP2, MPP3, MPP4, Mono: Monocyte, Neutro: Neutrocyte and MK: Megakaryocyte.
D, Violin plots of *Myct1*, *Esam* and *Vwf* expression in FL and ABM LT-HSC. Log2 values of the normalized read counts are represented.
E, Violin plots of *Spi1*, *Nfe2* and *Mpl* expression in FL and ABM LT-HSC. Log2 values of the normalized read counts are represented.
F, Heatmap hierarchical clustering centered on open chromatin peaks identified by ATACseq analysis in CTRL and iEG FL progenitors (LT-HSC+MPP1+MPP2) after 24h of Dox induction. Common: = peaks unchanged between CTRL and iEG; Down: = peaks lost or significantly reduced in iEG; Up: = peaks gained or significantly enriched in iEG. Windows of 11kb are shown. S: peak start, E: peak end.
G, Illustrations of ATAC-seq peaks in CTRL and iEG FL progenitors of representative common (*Rplp0*), Down (*Nfe2*) and Up (*Esam*) peaks using IGV software.
H, Pie chart illustrating the fraction of significantly deregulated genes in scRNAseq iEG vs. CTRL FL-HSC in which a modified EG peaks (either Up or Down) is present. The number of genes with a deregulated peak is indicated.
I, Histogram representation of the number of Common, Up and Down peaks between iEG FL progenitors, $CD41^+$ cell line or $Gr1^+$ cell line and CTRL FL progenitors.
J, Intensity profiles of Up peaks in FL progenitors described in (F) with CTRL and iEG FL progenitors, $CD41^+$ and $Gr1^+$ ATACseq data.
K, Motifs analysis under the peaks enriched in CTRL vs. iEG (Down peaks) in FL progenitor (peaks Down in iEG FL progenitors, dark grey), in iEG vs. CTRL (peaks Up in iEG FL progenitors, green), in megakaryoblastic $CD41^+$ (CD41, orange) and in myeloid $Gr1^+$ (Gr1, Blue) iEG cell lines. Chi2 analysis: GATA: FL vs. Down $p=3.46e^{-143}$, CD41 vs. Down $p=3.67e^{-316}$, Gr1 vs. Down $p=6.77e^{-68}$; ERG: FL vs. Down $p=1.19e^{-10}$, CD41 vs. Down $p=6.5e^{-32}$, Gr1 vs. Down $p=2.31e^{-15}$; PU.1: FL vs. Down p=0.21, CD41 vs. Down p=0.194, Gr1 vs. Down $p=5.39e^{-28}$; CEBP: FL vs. Down $p=1.12e^{-3}$, CD41 vs. Down $p=1.49e^{-22}$, Gr1 vs. Down $p=2.5e^{-201}$

Statistical significance is indicated as p values (Student's t test). *: p<0.05, **: p<0.01, ***: p<0.001.

Figure 6.
GATA and CEBPA activities functionally controls EG-induced phenotypes.
A, Quantitative RT-PCR analyses in LIN- CTRL and iEG FL14.5 and ABM-derived cells after 24h in liquid culture with Dox. Mean+/-SEM (n=3) is shown.
B, Quantitative RT-PCR analyses in CTRL and iEG ABM LT-HSC and MPP4-derived cells at P1. Mean+/-SEM (n=3) is shown.
C, Experimental design to ectopically express indicated TF in iEG ABM LT-HSC and MPP4.
D, Representative flow cytometry analyses of cells obtained at P1 after transduction of WT and iEG MPP4 with ERG, GATA1 or GFP-only retroviruses. Analysis was gated on GFP^+ cells.
E, Representative flow cytometry analyses of cells obtained at P1 after transduction of WT and iEG LT-HSC with SPI1, CEBPA or GFP-only retroviruses. Analysis was gated on GFP^+ cells.
F, Quantitative RT-PCR analyses in blasts from patients with AMKL (n=8, EG^- AMKL: empty circles, EG^+ AMKL: orange circles), AML (n=7, EG^- AMKL: empty squares, EG^+ AMKL: blue squares) and in the different blast populations from the dual phenotype ETO2-GLIS2$^+$ AML patient (#5) presented in Figure 1H ($CD41^-CD15^-$ immature: black triangle, $CD41^+CD15^-$ megakaryoblastic: orange triangle, $CD41^-CD15^+$ myeloid: blue triangle). Statistical significance is indicated as p values (Mann-Whitney test). *: p<0.05, **: p<0.01, ***: p<0.001.
G, Schematic representation of the bases for the pediatric and phenotypic specificities associated with ETO2-GLIS2 leukemia. Our data and published studies (22,26,23,24) support the idea that a shift from a higher megakaryoblastic potential (orange color) to a higher myeloid potential (blue color) in fetal vs. adult hematopoiesis is associated with a change in the GATA1 vs. CEBPA activities. Here we show that ETO2-GLIS2 imposes a stronger deregulation of self-renewal programs in fetal compared to adult hematopoiesis (including higher ERG and lower SPI1 activities). The combination of the basal transcriptional state controlling phenotypic output with a differential effect of ETO2-GLIS2 on self-renewal programs during hematopoietic ontogeny may therefore underlies the strong prevalence of acute megakaryoblastic leukemia (AMKL) in early childhood and more generally represent a basis for the specific pediatric and phenotypic incidence of human AMKL vs. other myeloid leukemia (AML) (lower part).
Statistical significance is indicated as p values (Student's t test) except otherwise mentioned. *: p<0.05, **: p<0.01, ***: p<0.001.

Figure 7.
ETO2-GLIS2 reversibly transforms LT-HSC.
A, Experimental design: purified LT-HSC and MPP cells from wild type (WT) or iEG mice expressing the Ubiquitin-GFP (GFP^+) were transplanted into wild-type Dox-treated recipients. Note that GFP expression is not Dox-dependent and therefore engraftment of all cells can be followed using GFP regardless of the Dox treatment.
B, Kaplan-Meier survival curve of recipients of naive iEG LT-HSC from ABM or FL, on Dox. Recipients were treated with Dox after transplantation. Log rank Mantel-Cox test iEG HSC FL vs. ABM recipients: p=0.0171. Median survival HSC ABM: 312d, HSC FL : 27d.
C, Kaplan-Meier survival plot of recipients of naive iEG MPP3 from ABM or FL kept on Dox. Log rank Mantel-Cox test iEG MPP3 FL vs. ABM recipients: p=0.0010. Median survival MPP3 FL: 33d.
D, Percentages of GFP^+ cells in BM, spleen weights, white blood cell (WBC) counts and platelet counts (Plt) in CTRL and iEG ABM HSC recipients and iEG FL HSC and MPP3 recipients. Spleen (CTRL vs. FL: p<0.0001, CTRL vs. ABM: p=0.0039), WBC (CTRL vs. FL: p=0.0095, CTRL vs. ABM: p=0.0309), Plt (CTRL vs. FL: p=0.0079, CTRL vs. ABM: p=0.1536).
E, Representative flow cytometry analysis of diseased recipients at time of sacrifice.
F, Histogram of the percentages of $CD41^+$ and $CD11b^+Gr1^+$ cells in the BM of primary diseased recipients. $CD41^+$ (CTRL vs. FL: p<0.0001, CTRL vs. ABM: p=0.0005), $CD11b^+Gr1^+$ (CTRL vs. FL: p=0.0016, CTRL vs. ABM: p=0.0717).

G, Histogram of the percentages of $B220^+$, $CD4^+$ and $CD8^+$ cells in the spleen of primary diseased recipients. $B220^+$ (CTRL vs. FL: p=0.012, CTRL vs. ABM: p=0.0102), T cells=$CD4^+$ or $CD8^+$ cells (CTRL vs. FL: p<0.0001, CTRL vs. ABM: p=0.0016).
H, Experimental design: $1x10^6$ BM cells from the diseased primary recipients at time of analysis were transplanted into secondary sub-lethally irradiated Dox-treated recipients. After two weeks, Dox treatment was maintained for group A (GFP^+ cells expressing iEG) and ceased in group B (GFP^+ cells lacking iEG expression).
I, Plt and RBC counts (top panels) and respective percentages of GFP^+ cells (lower panels) in secondary recipients of ABM LT-HSC-derived disease. D0: time at which Dox was maintained in group A and withdrawn in group B. Mean+/-SEM (n=6 / group) is shown.
J, Kaplan-Meier survival plot of secondary recipients transplanted with cells from diseased primary iEG ABM LT-HSC recipients. Secondary recipients were kept on Dox (Dox+) or not (Dox-). Log rank Mantel-Cox test Dox- vs. Dox+ recipients: p=0.0086.
K, Flow cytometry analyses in secondary recipients of iEG ABM LT-HSC-derived disease at six months after Dox withdrawal. Analyses were gated on GFP^+ (iEG donor-derived) or GFP^- (WT recipient) cells.
Statistical significance is indicated as p values (Student's t test except when otherwise specified). *: p<0.05, **: p<0.01, ***: p<0.001.

A

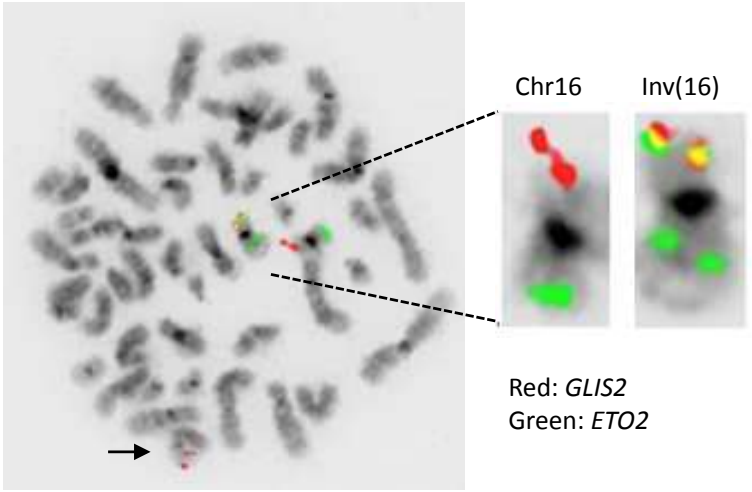

B

Phenotype	EG$^+$	Total	%
AMKL	8	34	23.5%
AML M0-5	5	242	2.1%
All AML	13	276	4.7%

C

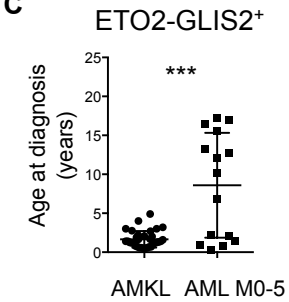

D

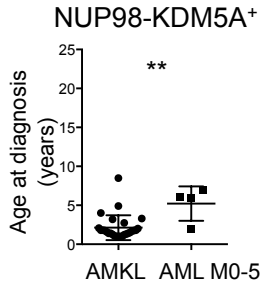

E

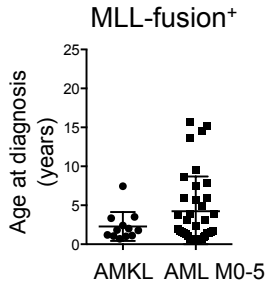

F

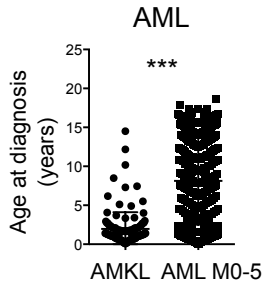

G

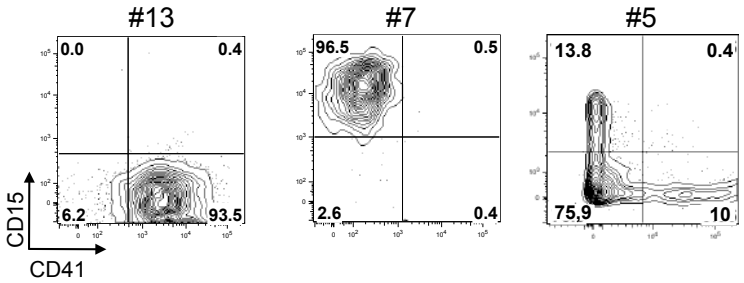

H

I

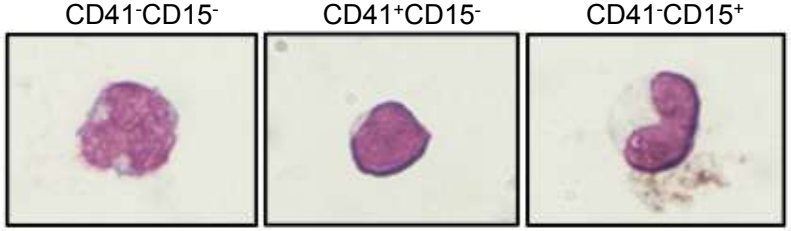

J

Patient	Population	Engrafted
#13	CD34$^+$CD41$^+$	6/6
#5	CD15$^-$CD41$^-$	6/6
	CD15$^+$CD41$^-$	0/6
	CD41$^+$CD15$^-$	0/5

K

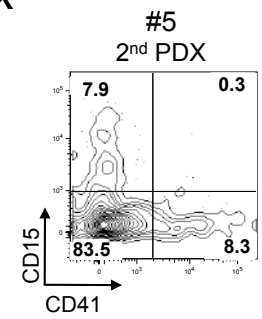

Figure 1

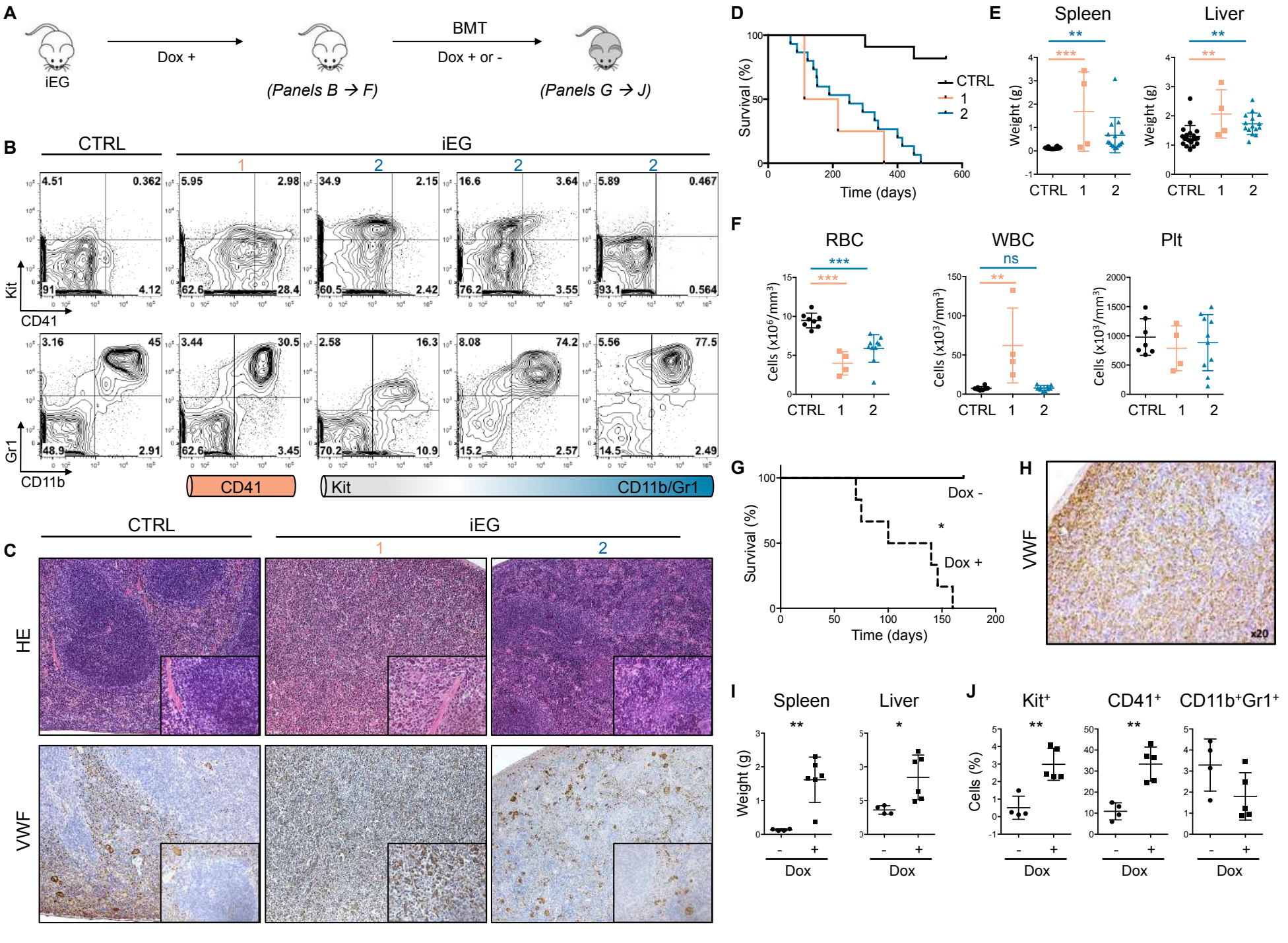
A
iEG
Dox +
(Panels B → F)
BMT
Dox + or -
(Panels G → J)
B
CTRL
iEG
1
2
2
2
Kit
CD41
Gr1
CD11b
CD41
Kit
CD11b/Gr1
C
CTRL
iEG
1
2
HE
VWF
D
Survival (%)
Time (days)
CTRL
1
2
E
Spleen
Liver
Weight (g)
CTRL 1 2
F
RBC
WBC
Plt
Cells (x10⁶/mm³)
Cells (x10³/mm³)
ns
G
Survival (%)
Time (days)
Dox -
Dox +
H
VWF
x20
I
Spleen
Liver
Weight (g)
Dox
J
Kit⁺
CD41⁺
CD11b⁺Gr1⁺
Cells (%)
Dox

Figure 2

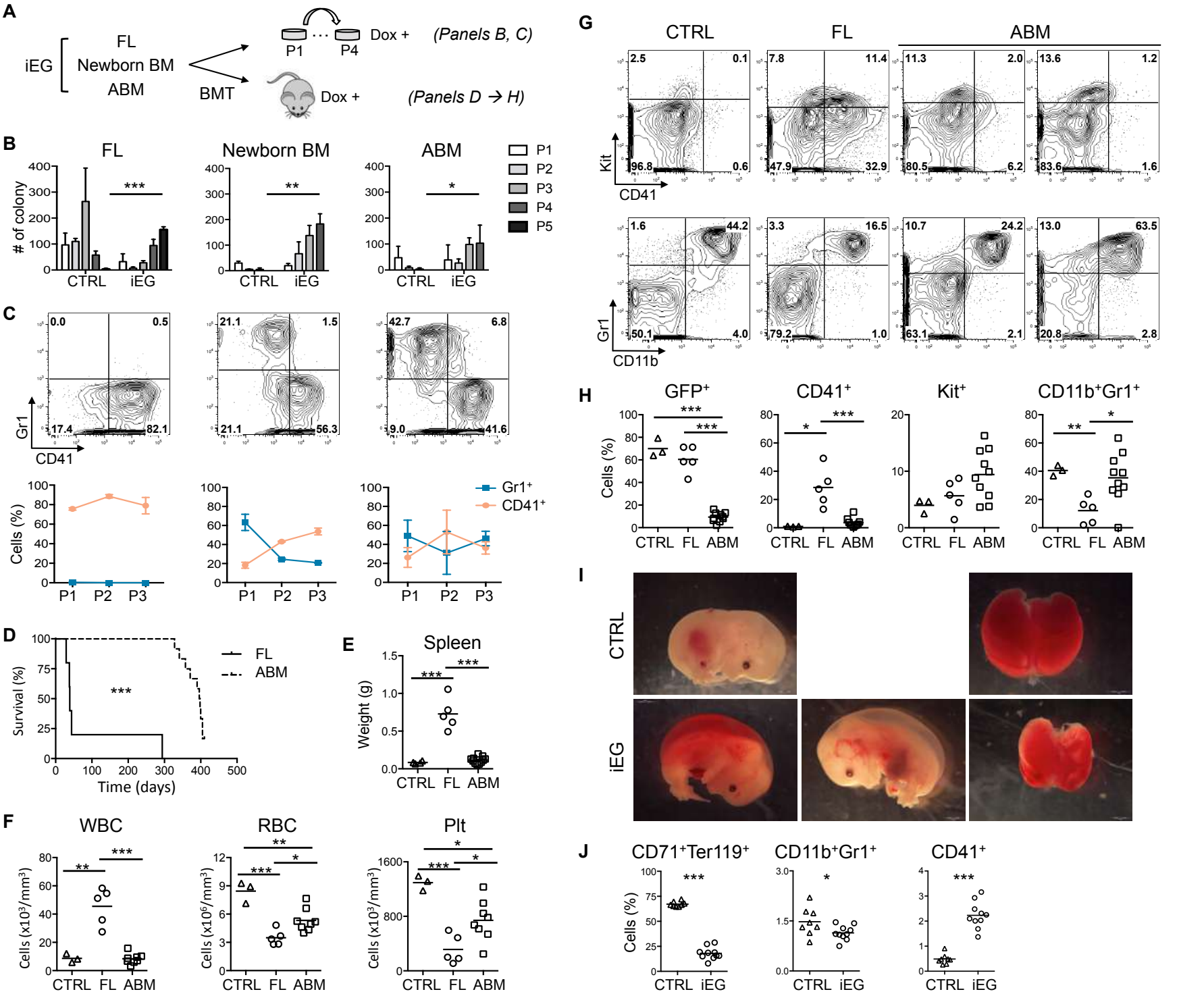
A
iEG
FL
Newborn BM
ABM
BMT
P1
P4
Dox +
(Panels B, C)
Dox +
(Panels D → H)
B
FL
Newborn BM
ABM
P1
P2
P3
P4
P5
# of colony
CTRL
iEG
C
Gr1
CD41
Cells (%)
Gr1+
CD41+
D
Survival (%)
Time (days)
FL
ABM
E
Spleen
Weight (g)
F
WBC
RBC
Plt
Cells (x10³/mm³)
Cells (x10⁶/mm³)
G
CTRL
FL
ABM
Kit
CD41
Gr1
CD11b
H
GFP+
CD41+
Kit+
CD11b+Gr1+
I
CTRL
iEG
J
CD71+Ter119+
CD11b+Gr1+
CD41+

Figure 3

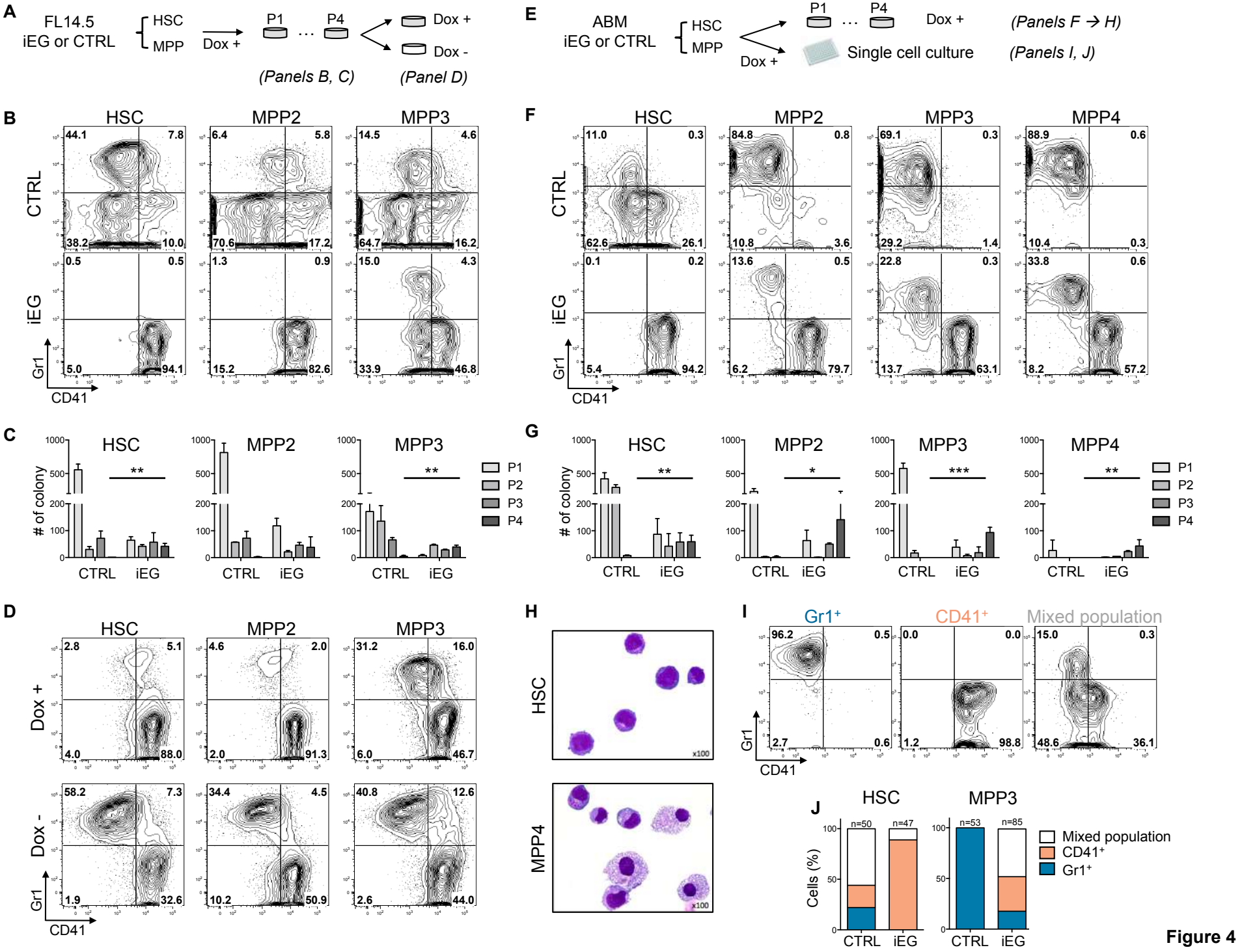
A
FL14.5
iEG or CTRL
HSC
MPP
Dox +
P1
P4
Dox +
Dox -
(Panels B, C)
(Panel D)
E
ABM
iEG or CTRL
HSC
MPP
Dox +
P1
P4
Dox +
Single cell culture
(Panels F → H)
(Panels I, J)
B
HSC
MPP2
MPP3
CTRL
iEG
Gr1
CD41
44.1
7.8
38.2
10.0
6.4
5.8
70.6
17.2
14.5
4.6
64.7
16.2
0.5
0.5
5.0
94.1
1.3
0.9
15.2
82.6
15.0
4.3
33.9
46.8
F
HSC
MPP2
MPP3
MPP4
11.0
0.3
62.6
26.1
84.8
0.8
10.8
3.6
69.1
0.3
29.2
1.4
88.9
0.6
10.4
0.3
0.1
0.2
5.4
94.2
13.6
0.5
6.2
79.7
22.8
0.3
13.7
63.1
33.8
0.6
8.2
57.2
C
HSC
MPP2
MPP3
# of colony
CTRL
iEG
**
**
**
P1
P2
P3
P4
G
HSC
MPP2
MPP3
MPP4
# of colony
**
*
***
**
P1
P2
P3
P4
D
HSC
MPP2
MPP3
Dox +
Dox -
Gr1
CD41
2.8
5.1
4.0
88.0
4.6
2.0
2.0
91.3
31.2
16.0
6.0
46.7
58.2
7.3
1.9
32.6
34.4
4.5
10.2
50.9
40.8
12.6
2.6
44.0
H
HSC
MPP4
x100
x100
I
Gr1+
CD41+
Mixed population
Gr1
CD41
96.2
0.5
2.7
0.6
0.0
0.0
1.2
98.8
15.0
0.3
48.6
36.1
J
HSC
MPP3
n=50
n=47
n=53
n=85
Cells (%)
CTRL
iEG
Mixed population
CD41+
Gr1+

Figure 4

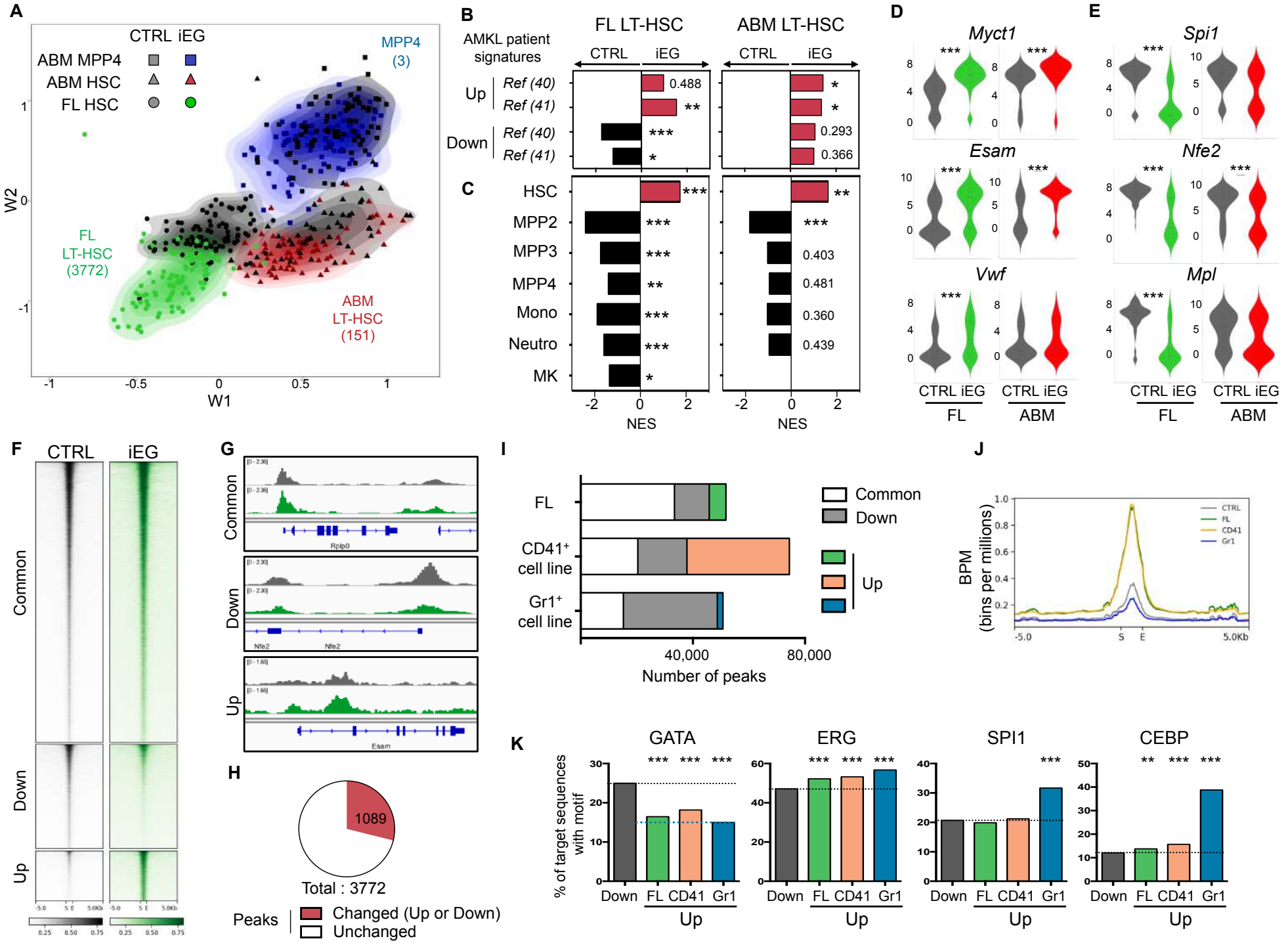
A
CTRL iEG
ABM MPP4
ABM HSC
FL HSC
MPP4 (3)
FL LT-HSC (3772)
ABM LT-HSC (151)
W1
W2
B
AMKL patient signatures
FL LT-HSC
ABM LT-HSC
CTRL
iEG
Up
Down
Ref (40)
Ref (41)
0.488
0.293
0.366
C
HSC
MPP2
MPP3
MPP4
Mono
Neutro
MK
0.403
0.481
0.360
0.439
NES
D
Myct1
Esam
Vwf
E
Spi1
Nfe2
Mpl
CTRL iEG
FL
ABM
F
CTRL
iEG
Common
Down
Up
G
Common
Down
Up
Rplp0
Nfe2
Esam
H
1089
Total : 3772
Peaks
Changed (Up or Down)
Unchanged
I
FL
CD41+ cell line
Gr1+ cell line
Common
Down
Up
40,000
80,000
Number of peaks
J
BPM (bins per millions)
CTRL
FL
CD41
Gr1
-5.0
S
E
5.0Kb
K
GATA
ERG
SPI1
CEBP
% of target sequences with motif
Down
FL
CD41
Gr1
Up

Figure 5

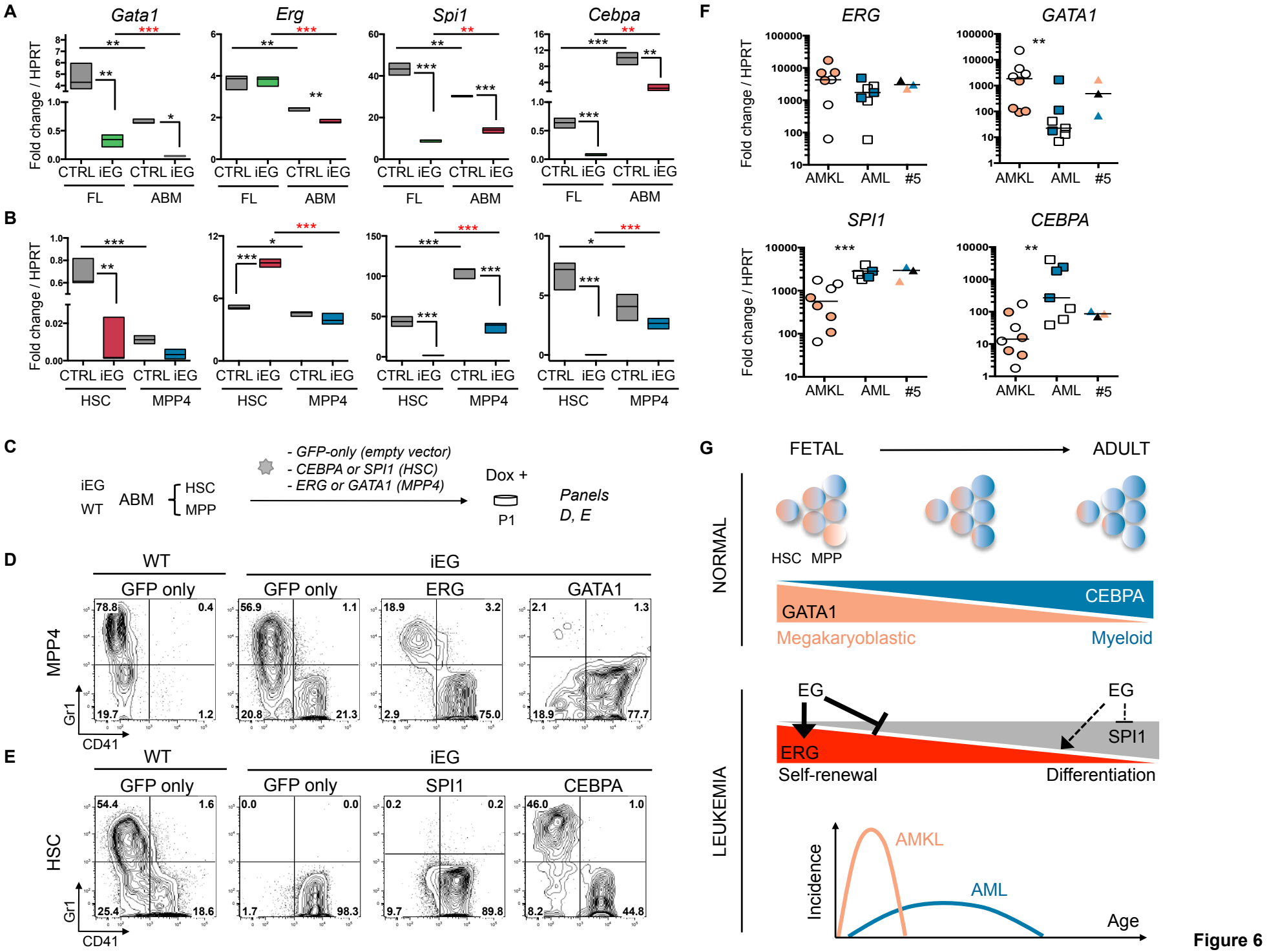
A
Gata1
Erg
Spi1
Cebpa
Fold change / HPRT
CTRL iEG CTRL iEG
FL
ABM
B
HSC
MPP4
C
iEG
WT
ABM
HSC
MPP
- GFP-only (empty vector)
- CEBPA or SPI1 (HSC)
- ERG or GATA1 (MPP4)
Dox +
P1
Panels
D, E
D
WT
iEG
GFP only
ERG
GATA1
MPP4
Gr1
CD41
78.8
0.4
19.7
1.2
56.9
1.1
20.8
21.3
18.9
3.2
2.9
75.0
2.1
1.3
18.9
77.7
E
SPI1
CEBPA
HSC
54.4
1.6
25.4
18.6
0.0
0.0
1.7
98.3
0.2
0.2
9.7
89.8
46.0
1.0
8.2
44.8
F
ERG
GATA1
SPI1
CEBPA
AMKL
AML
#5
G
FETAL
ADULT
NORMAL
HSC MPP
GATA1
CEBPA
Megakaryoblastic
Myeloid
LEUKEMIA
EG
EG
ERG
SPI1
Self-renewal
Differentiation
Incidence
AMKL
AML
Age

Figure 6

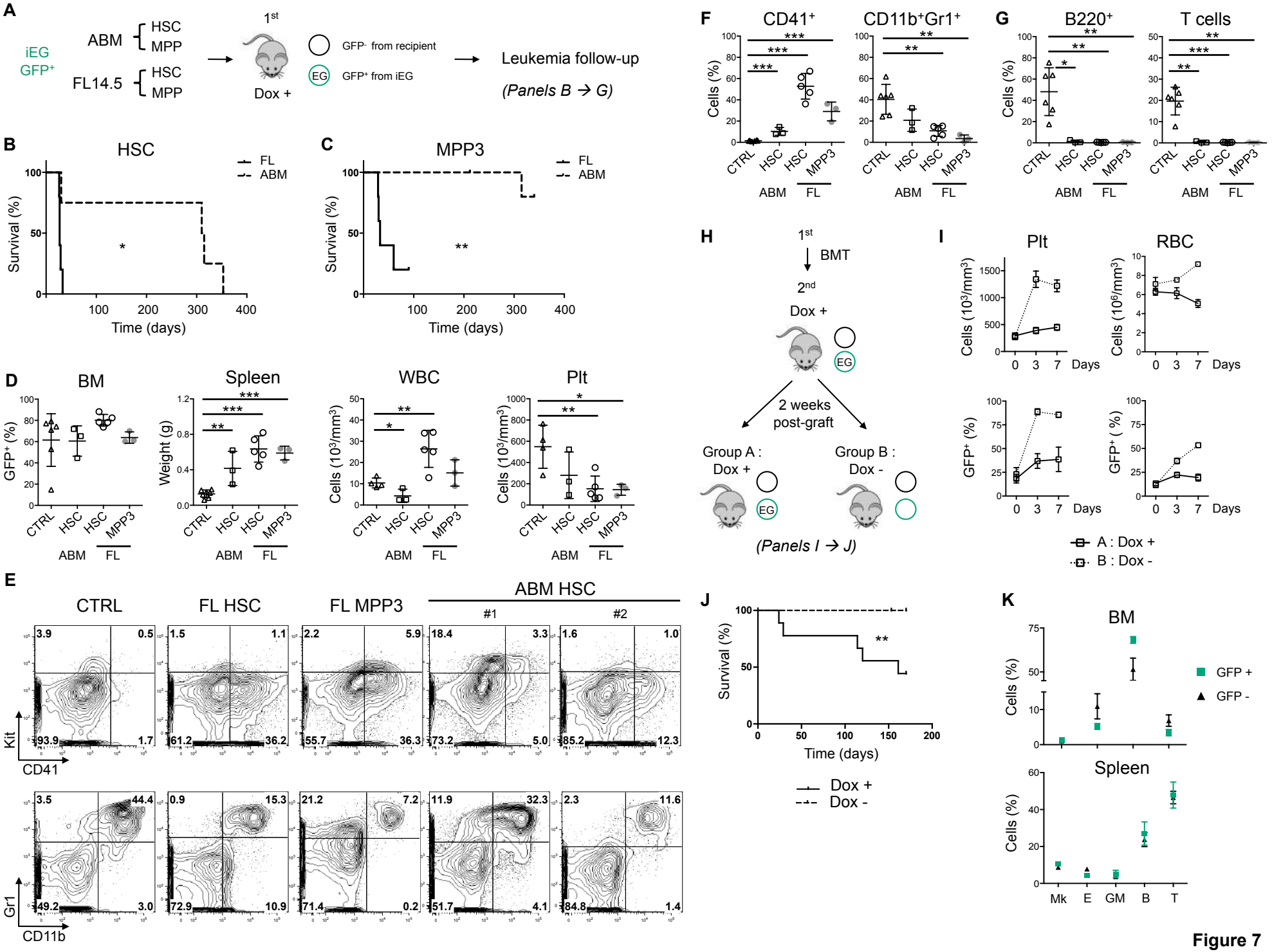
A
iEG GFP+
ABM HSC MPP
FL14.5 HSC MPP
1st
Dox +
GFP- from recipient
EG GFP+ from iEG
Leukemia follow-up
(Panels B → G)
B
HSC
FL
ABM
Survival (%)
Time (days)
C
MPP3
D
BM
Spleen
WBC
Plt
GFP+ (%)
Weight (g)
Cells (10³/mm³)
CTRL HSC HSC MPP3
ABM FL
E
CTRL
FL HSC
FL MPP3
ABM HSC
#1
#2
Kit
CD41
Gr1
CD11b
F
CD41+
CD11b+Gr1+
G
B220+
T cells
Cells (%)
H
1st
BMT
2nd
Dox +
EG
2 weeks post-graft
Group A : Dox +
Group B : Dox -
(Panels I → J)
I
Plt
RBC
Cells (10³/mm³)
Cells (10⁶/mm³)
GFP+ (%)
GFP+ (%)
Days
A : Dox +
B : Dox -
J
Survival (%)
Time (days)
Dox +
Dox -
K
BM
Spleen
Cells (%)
GFP +
GFP -
Mk E GM B T

Figure 7